

Relocation of the 1982 Miramichi, New Brunswick, Canada, aftershock sequence

Shutian Ma¹ and Dariush Motazedian¹

¹Carleton University

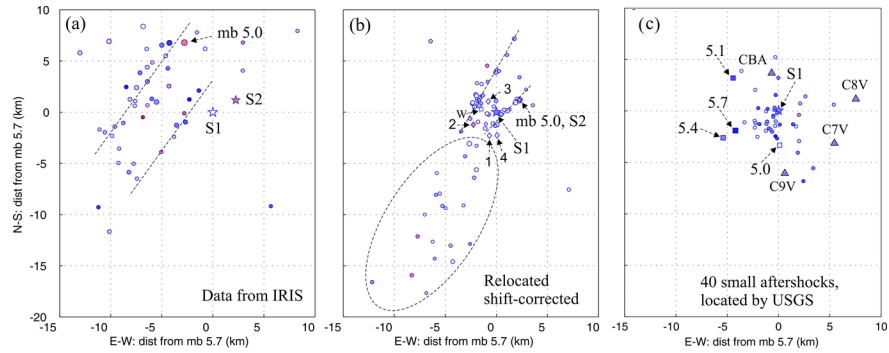
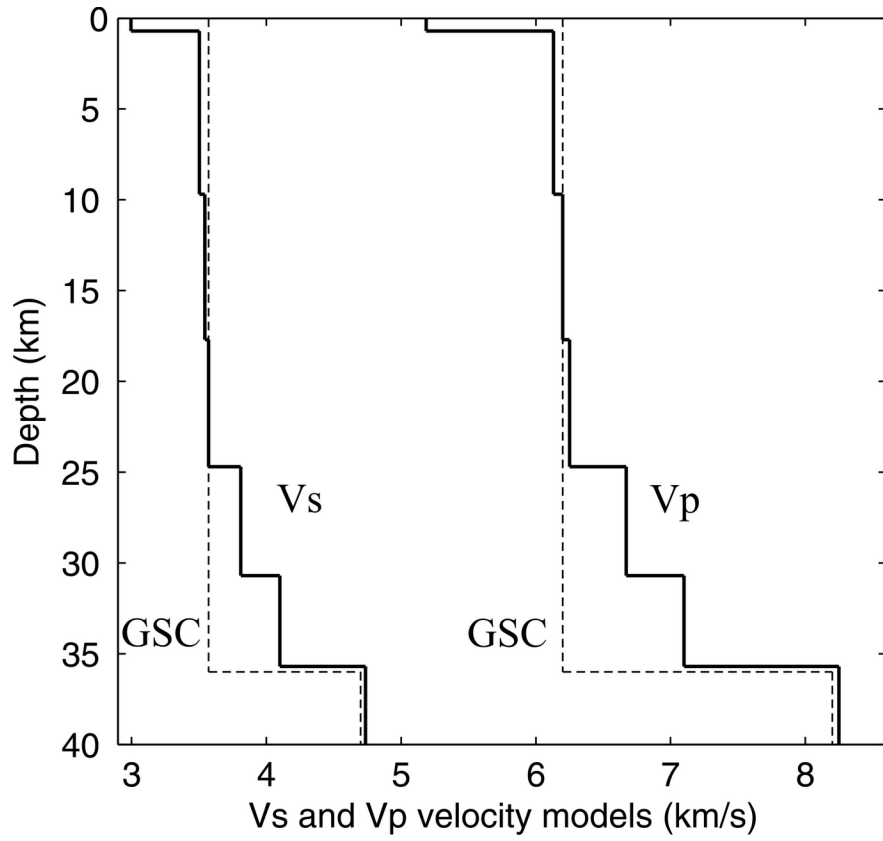
November 22, 2022

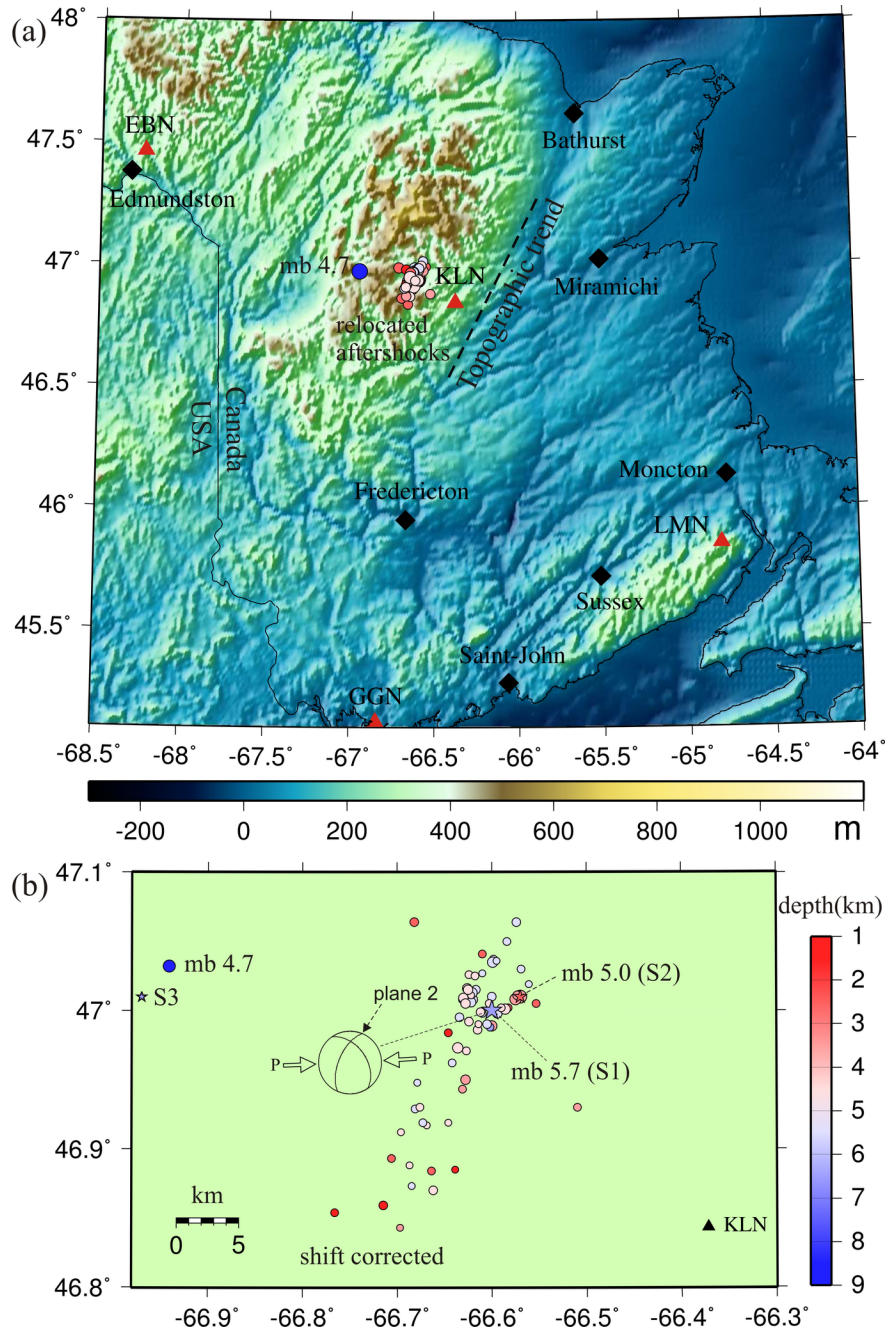
Abstract

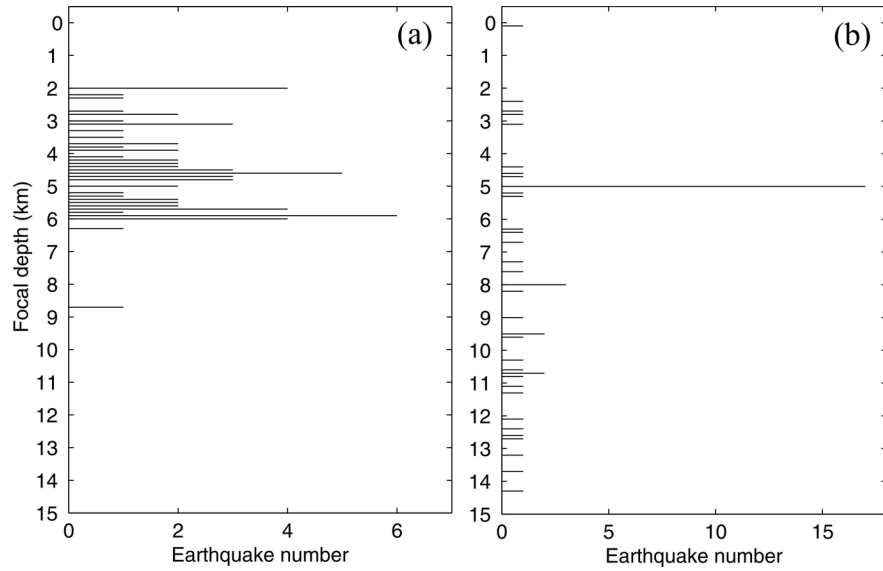
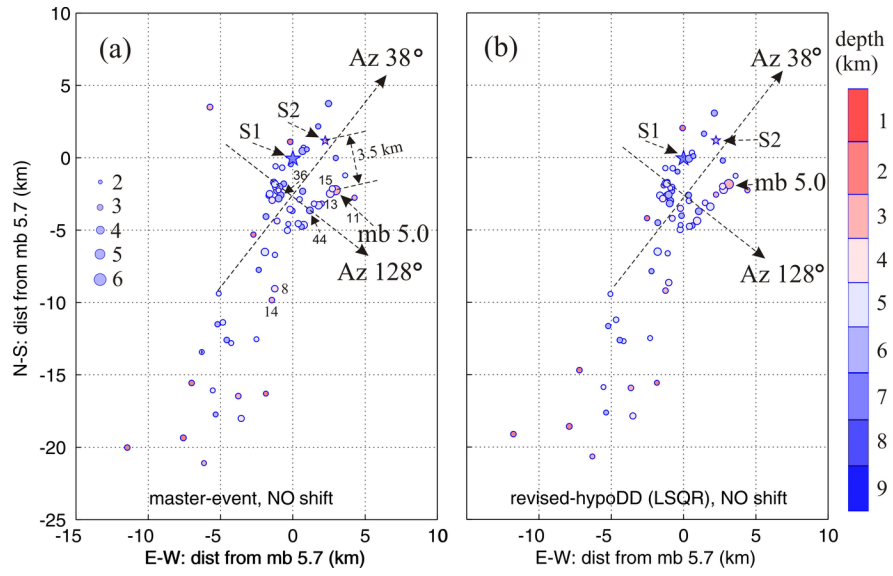
On 9 January 1982, in the Miramichi region of New Brunswick, Canada, an earthquake with body-wave magnitude (mb) 5.7 occurred. It was followed by extensive aftershocks and felt throughout eastern Canada and northeastern USA. Digital seismic stations were not yet common by 1982. Fortunately, three stations (KLN, EBN and GGN) produced excellent waveform records for the larger aftershocks allowing these aftershocks to be relocated. For each aftershock, its focal depth was first determined using the depth phase sPg; then, with depth fixed, the epicenter was determined using a set of arrival times recorded for the Pg-, Sg-, and Pn-phases at the three stations. Sixty-eight aftershocks were relocated; most of them occurred in a 5×5 km area and with depths of 2 to 6 km. The epicentres formed two linear trends in the NE-SW direction. The trends were close to the northeast strike of the focal mechanism of the mainshock and consistent with the topographic trend near the source region. A gap between the trends separated the epicenters into two groups. One group represents the rupture area caused by the mainshock, and the other group might represent the rupture area caused by the mb 5.4 principal aftershock.

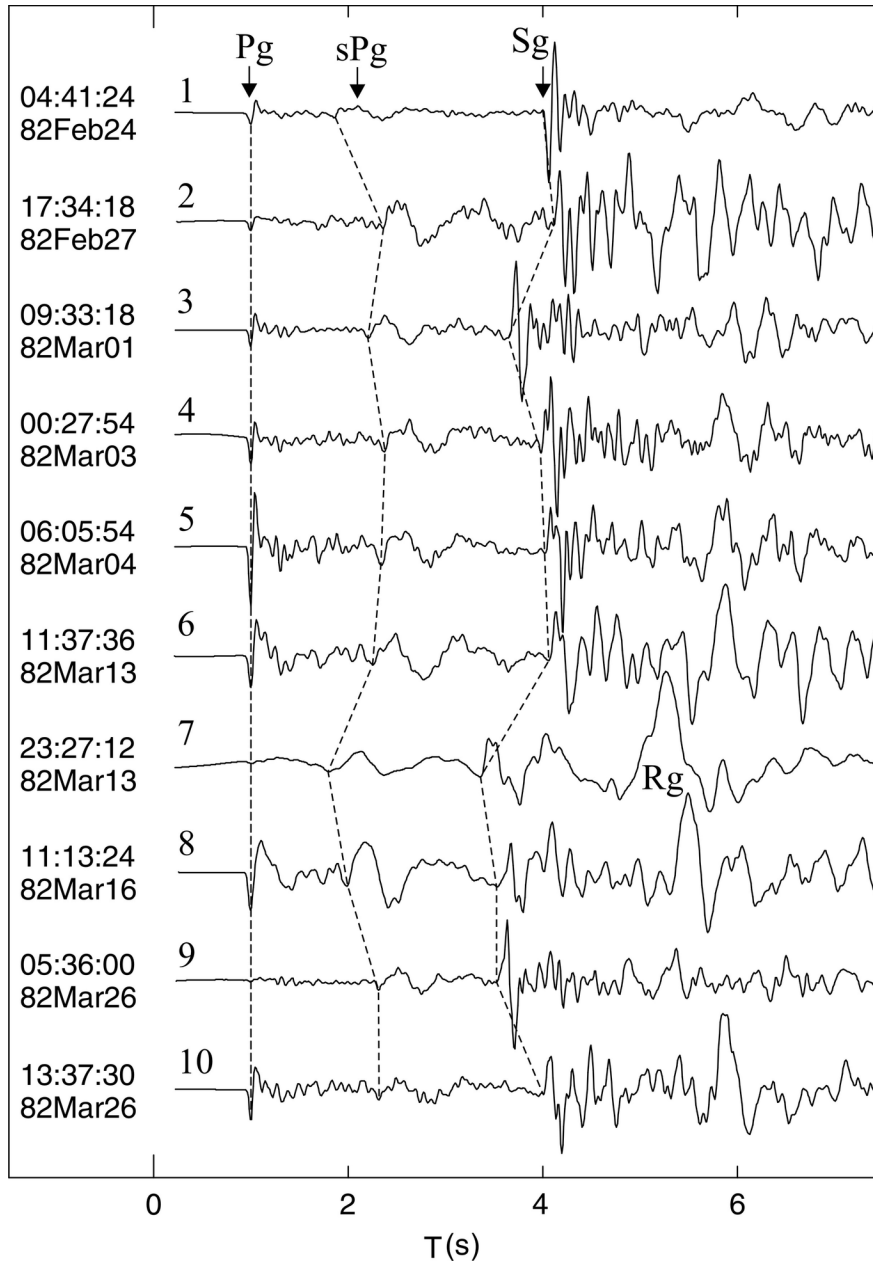
Hosted file

essoar.10510226.1.docx available at <https://authorea.com/users/538683/articles/599669-relocation-of-the-1982-miramichi-new-brunswick-canada-aftershock-sequence>









Relocation of the 1982 Miramichi, New Brunswick, Canada, aftershock sequence
Dariush Motazedian¹ and Shutian Ma²

¹Department of Earth Sciences, Carleton University

1125 Colonel By Drive

Ottawa, Ontario, K1S 5B6, Canada

Dariush.Motazedian@Carleton.ca

(D.M.)

²Department of Earth Sciences, Carleton University

1125 Colonel By Drive

Ottawa, Ontario, K1S 5B6, Canada

shutian33@yahoo.ca

(S.M.)

Revised Dec 2021

Corresponding author: Shutian Ma; shutian33@yahoo.ca

Abstract:

On 9 January 1982, in the Miramichi region of New Brunswick, Canada, an earthquake with body-wave magnitude (mb) 5.7 occurred. It was followed by extensive aftershocks and felt throughout eastern Canada and northeastern USA. Digital seismic stations were not yet common by 1982. Fortunately, three stations (KLN, EBN and GGN) produced excellent waveform records for the larger aftershocks allowing these aftershocks to be relocated. For each aftershock, its focal depth was first determined using the depth phase sPg ; then, with depth fixed, the epicenter was determined using a set of arrival times recorded for the Pg -, Sg -, and Pn -phases at the three stations. Sixty-eight aftershocks were relocated; most of them occurred in a 5×5 km area and with depths of 2 to 6 km. The epicenters formed two linear trends in the NE-SW direction. The trends were close to the northeast strike of the focal mechanism of the mainshock and consistent with the topographic trend near the source region. A gap between the trends separated the epicenters into two groups. One group represents the rupture area caused by the mainshock, and the other group might represent the rupture area caused by the mb 5.4 principal aftershock.

1. Introduction

The 9 January 1982 Miramichi, New Brunswick, magnitude (mb) 5.7 earthquake was a rare case in North America. It was felt throughout eastern Canada and northeastern USA and intrigued scientists and the public as it was the largest one in eastern Canadian and eastern US for 40 years. The mainshock (mb 5.7;

M_W 5.6) occurred at 1253 UT on the 9th January, followed 3.5 hours later by a mb 5.1 (M_W 4.9) principal aftershock. On the January 11th the second principal aftershock (mb 5.4, M_W 5.0) followed, then on March 31st the third principal aftershock (mb 5.0, M_W 4.9) occurred.

The mb magnitude was used for the mainshock and the three principal aftershocks in the majority of the publications and the media for many years. The moment magnitudes can be found in the report by Bent (2015). For convenience (and because they have had variously-reported magnitude values and types in the past), we refer to the four earthquakes as S1, S2, S3 and S4 respectively. That the mainshock has three principal aftershocks is also a rare case throughout the world, so the three principal aftershocks were also study topics.

Three field surveys were conducted in 1982 by the Geological Survey of Canada (GSC) to investigate the aftershock sequence. In the January survey, the most detailed coverage of the aftershock activity was from 19 to 22 January (the temperatures were below -25°C) when aftershocks were recorded by analog MEQ-800 seismographs at four sites within 10 km of the active zone. The hypocenter of the mainshock was estimated using the hypocenters of the detected small aftershocks. The April survey was conducted in response to the 31 March mb 5.0 principal aftershock, whose hypocenter was also estimated using the hypocenters of the detected small aftershocks. The survey in June followed the 16 June mb 4.7 earthquake [Figure 1(b)]. As this event was located about 30 km west of the Miramichi mainshock (e. g. Wetmiller et al. 1984), it is not discussed in this article.

Responding to a request from Canada, the U.S. Geological Survey (USGS) installed a portable digital network. This network located about 40 aftershocks between January 15 to 22, 1982 (Cranswick et al., 1982). Among the 40 aftershocks, 4 larger ones were relocated and their focal mechanisms were studied by Saikia and Herrmann (1985).

The focal mechanism of the mainshock was also studied. It was a thrust type (e.g., Basham and Adams, 1984). The rupture was inferred to be updip on a west dipping NNE striking fault plane (Choy et al., 1983). The “beach-ball” is plotted in Figure 1 (b) using gCMT data (the global CMT project; globalcmt.org), and the inferred rupture plane is labelled “plane 2”.

As this earthquake sequence occurred in an almost completely uninhabited region, the damage was minor. However, investigating this mainshock and its aftershocks is important for understanding intraplate seismic activity.

Since there was no close Canadian digital seismic station, a new station (KLN) was installed by GSC on 23 January 1982 (14 days after the mainshock and about 25 km away because of logistical constraints) to better monitor the sequence. The station was one of the Eastern Canadian Telemetered Network (ECTN). KLN recorded hundreds of aftershocks, and the waveform record quality was excellent. Two existing ECTN stations, EBN and GGN, also had clear

records for the larger aftershocks ($m_N \geq 2.8$). Figure 1 (a) shows the distributions of these three stations.

Between latitudes $46.88^\circ \text{ N} - 47.16^\circ \text{ N}$ and longitudes $66.35^\circ \text{ W} - 66.80^\circ \text{ W}$, there were about 700 aftershocks (the smaller aftershocks detected in the field surveys are not included) in the GSC catalogue database as of the end of 2016. These represent aftershocks large enough to be determined from the ECTN and its successor during routine analysis. The seismic activity is still ongoing. Ma and Motazedian (2017) determined the focal depths for more than 100 aftershocks with $m_N \geq 2.8$, using depth phase sPmP recorded at EBN, but left the epicenters unchanged. Most of the aftershocks in the database were assigned the same epicenter (47.00° N , 66.60° W), that of the mainshock, determined from the distribution of the small aftershocks, detected during the January 1982 field survey (Wetmiller et al., 1984).

For an earthquake with Pg and Sg arrival readings at KLN, Pg at EBN, and Pn at GGN, a conventional location method can in principle be used to determine its hypocenter. However, an earthquake's focal depth is usually much smaller than epicentral distance to the recording stations, so the travel time contribution of the depth is typically much smaller than that of the station distance. As such, the error (uncertainty) in the depth is much larger than the uncertainties in the latitude and longitude of an epicenter. To reduce the error in an epicenter, a focal depth can be first determined using a depth phase; then, the epicenter can be relocated using that depth.

Since the station coverage for the sequence was not good (Figure 1), and regional velocity models are poor, it was not possible to determine an epicenter for an aftershock with small absolute errors. However, errors in the relative locations in a small aftershock group should be smaller and can be obtained using a master-event method (e.g., Havskov and Ottemöller, 2010).

The mb 5.7 mainshock had three principal aftershocks: mb 5.1 occurred on 9 January, mb 5.4 on 11 January, and mb 5.0 on 31 March. The three aftershocks were relocated by Choy et al. (1983) (their Fig. 11). Because the energy released by the mb 5.4 aftershock is of the same order as that of the mainshock, the Miramichi earthquake is also called a double-earthquake. The focal depths of the mainshock and its three principal aftershocks were determined using a waveform modeling method (Ma and Motazedian, 2017). The depth of mb 5.7 was 6.8 km, mb 5.1, 5.5 km, mb 5.4, 5.2 km, and mb 5.0, 2.0 km. The depths were progressively shallower with occurrence times.

Our motivation was to obtain a hypocentral distribution by relocating larger aftershocks using the phase arrival readings at the three stations mentioned above. In the following we analyze the waveform data, introduce the methods for relocating aftershocks, present the hypocentral distribution features of the relocated aftershocks, compare the 68 relocated hypocenters with those from other sources, and discuss some related issues.

2. Waveform data analysis

The closest station to the sequence (about 25 km) was KLN (Figure 1). KLN had clear Pg- and Sg-phase records for almost all aftershocks. Note that the Sg phase was read off the vertical component and that the velocity traces were converted into displacement traces. Figure 2 shows the seismograms generated by 10 aftershocks. The onsets of the Pg and Sg phases are clear on all 10 traces; Rg can be seen on some, confirming that they are shallow.

The second closest station was EBN (about 135 km from the sequence). At EBN, the onset of the Pg phase was usually clear on the seismograms generated by aftershocks with $m_N \approx 2.8$, so the arrival time of the Pg phase could be measured. For example, Figure 3 shows three records at EBN. However, the onset of Sg is not clear on these vertical seismograms, and its arrival time cannot be accurately measured. The horizontal dashed line with two arrows indicates the S-wave train.

The third closest station was GGN (station distance ~ 200 km). At this station, the Pn phase (any P wave bottoming in the uppermost mantle or an upgoing P wave from a source in the uppermost mantle; it can be the first arrival at a regional station beyond the cross-over distance), generated by aftershocks with $m_N \approx 2.8$, was clear. Similar to the records at EBN (Figure 3), there were no clear Sg-wave arrivals at GGN. Figure 4 shows P-wave segments at GGN that were generated by five aftershocks.

The waveforms at station LMN (station distance ~ 200 km; Figure 1) were also analyzed. The Pn phase, generated by aftershocks with $m_N \approx 2.8$, was clear when the seismograph at this station operated normally. Unfortunately, in 1982, the seismograms at LMN were often rectangular pulses with different amplitudes (probably due to instrument malfunction), so the Pn arrival times could only be measured for some aftershocks. As such, the waveform records were not used in the relocations.

During the studies on the focal depths for the larger aftershocks in the Miramichi sequence, Ma and Motazedian (2017) found that the time differences between the Sg and Pg phases recorded at KLN from different aftershocks were not consistent. Some of the differences were similar, but some were not. Figure 2 presents seismograms generated by the first 10 aftershocks listed in Table 1. For each aftershock, its hypocentral distance to KLN is mainly constrained by the time difference $T_{Sg} - T_{Pg}$, while its depth is constrained by $T_{sPg} - T_{Pg}$. Thus, the different onsets of the Pg, sPg, and Sg phases show that the aftershocks generating the seismograms have different hypocenters. Counting from the top, the times between Sg and Pg and between sPg and Pg of the fourth and fifth traces are almost the same; these similarities imply that the two aftershocks that generated these two records have similar focal depths and epicentral distances. The noticeably different Pg/Sg amplitude ratios between these two records imply that the two aftershocks have different focal mechanisms and/or locations.

3. Methods

To obtain a reliable hypocentral distribution using very limited waveform

records, we used several modern techniques. In this section, we briefly introduce the revised hypoDD technique, a master-event relocation method, and the depth phase modeling method.

3.1. The revised-hypoDD technique

Waldhauser and Ellsworth (2000) presented a double-difference technique, known as hypoDD. Their method can simultaneously relocate a large number of earthquakes and can dramatically improve the precision of event relative locations. Despite such technical advances, focal depths are typically the least well-resolved hypocentral parameters because the location method uses arrival times of P- and S-waves that are primarily controlled by epicentral distance rather than focal depth. Ma and Eaton (2011) made a revision to the original hypoDD by removing the depth column in the DD equations and providing a well-determined focal depth to each event in the initial input data. The unknown parameters were dropped from 4 to 3 for each event.

To prevent an ill-conditioned system of DD-equations, hypoDD ensures connectivity between events by grouping events into clusters, with each cluster having a chain of links from any event to any other event in the cluster. The strength of this chain is defined by a minimum number of observations per event pair that build up the chain. Typical thresholds are similar to the number of degrees of freedom for an event pair, which is 8 (the epicenter, focal depth, and origin time; Waldhauser, 2001).

For the Miramichi sequence, only 4 arrival time readings are available for each aftershock (Pg and Sg at station KLN, Pg at EBN, and Pn at GGN). According to the hypoDD manual (Waldhauser, 2001), the original hypoDD cannot be used to relocate the Miramichi aftershocks. For the revised-hypoDD, 6 unknown parameters in each event pair must be solved. As the unknown parameters become fewer, the requirements for the observed data become less onerous, and the revised-hypoDD may be able to relocate the Miramichi aftershocks. However, we preferred to use a master-event method to relocate the Miramichi aftershocks because we had no previous experience in using the revised-hypoDD to relocate clusters for which observations are very limited.

3.2. A master-event relocation method

Master-event relocation methods have been studied and used by many scientists (e.g., Stoddard and Woods, 1990; Zollo et al., 1995; Havskov and Ottemöller, 2010; Bouchaala, et al., 2013). The events in a group can be relocated relative to one particularly well-located event. This particular event is called the master event (ME), while the others in the group are called secondary events or slave events (SE). The relative locations between events in an earthquake group can be determined with greater accuracy than the absolute location of any event in the group.

A P-phase or S-phase traveling from an earthquake in a group to a station spends most time outside the group region. For a specific phase at the same station,

the difference (residual) between the observed and calculated travel times of the ME is approximately equal to those of the SEs. Using the residuals of the ME as station corrections to SEs, the locations of the SEs are made relative to the ME because all relative changes in travel times are now entirely due to the changes in earthquake locations within the region.

The formulas in the master-event method provided by Bouchaala et al. (2013) are as follows:

$$(1)$$

$$(2)$$

where are differential travel times of phase k , i is an index for a SE, and obs and cal mean observed and calculated, respectively. Formula 1 changes as follows to use a conventional event locating program to relocate the ME and SEs:

$$= (3)$$

where denotes the origin time of the SE i , indicates the origin time of the ME, and and denote the arrival times of phase k for the SE i and the ME, respectively.

In the master-event method, the residual of phase k is a constant for all SEs. Formula (3) could be changed to

$$(4)$$

The residual could be treated as station corrections in an input file for a conventional event locating program (Havskov and Ottemöller, 2010).

The steps in the master-event method described by Havskov and Ottemöller (2010) are as follows:

(1) Locate the ME. The ME must show clear phase arrivals to determine a reliable hypocenter using a conventional location routine and is therefore chosen based on the seismograms' signal-to-noise ratios and sharp first arrivals at all stations (Fremont and Malone, 1987).

(2) Select stations and phases which are common to the ME and SEs. This step is necessary in the master-event method.

(3) Calculate the residuals at the selected stations for the ME; a residual is the difference between the observed arrival time of a phase and that of the corresponding synthetic phase. The obtained residuals are the station corrections for the SEs.

(4) Add the residual of a certain phase to the arrival time readings of the same phase for the ME and SEs.

(5) Relocate all events (the ME and the SEs; possibly fix depth) using a conventional event locating program. We used the hypocenter location program in SEISAN (e.g., Havskov and Ottemöller, 1999).

3.3.A depth phase modeling procedure to determine a focal depth

When the Pg- and Sg-phase arrival times at KLN, Pg at EBN, and Pn at GGN are available for an aftershock in the sequence, theoretically, the four source parameters (origin time, latitude, longitude, and focal depth) can be determined for the aftershock using the above four arrival time readings. However, the uncertainty in the four parameters could be large, especially that for focal depth. In practice, if only a few arrival time readings are available or station coverage is poor, the focal depth is assigned a nominal value to stabilize the location when locating an event.

To reduce uncertainties in epicenters due to uncertainty in focal depth, the time difference along a trace between depth phase sPg and its reference phase Pg (Figure 2) can be used to retrieve a reliable focal depth for the aftershock that generated the trace; then, the epicenter of the aftershock can be relocated at the focal depth retrieved. In this way, the trade-off between the epicenter and the focal depth is removed, so the uncertainty in the epicenter is dramatically reduced.

The crucial step in the procedure to retrieve a focal depth using a depth phase is the generation of the synthetic traces along which the depth phase appears. In generating synthetic waveforms, a crustal model, earthquake location, focal mechanism, and focal depth are needed input parameters for a computer program. Because the crustal structures through which the waves travel are related to travel times, the crustal model is a key parameter in generating synthetic depth phases. The reflectivity method (Randall, 1994), the centroid moment tensor solution for the Miramichi mainshock from the gCMT Catalog (see data and resources section), and the crustal model introduced in next section were used to generate the synthetic traces. The details of the depth phase studies can be found in e.g., Langston (1987), Uski et al. (2003), Ma and Atkinson (2006), and Ma (2010).

4. Crustal Model

There are several studies on crustal models for eastern Canada (e.g., Mereu et al., 1986; Motazedian et al., 2013). Rayleigh-wave dispersion data from the 23 June 2010 M_W 5.2 earthquake about 60 km northeast of Ottawa, Ontario, were used to obtain 14 crustal velocity models around the epicenter (Motazedian et al., 2013). The Rayleigh wave travel paths for model No. 8 ran approximately through the Miramichi region.

In addition, in recent years, some shallow, small earthquakes occurred in the Miramichi region. Those small earthquakes generated Rg-wave records. Using the Rg-wave dispersion data, models for the shallow part of the crust (0–10 km) were obtained (Ma, 2015). A velocity model was formed for the Miramichi region (Figure 5) by replacing the shallow part of the model by Motazedian et al. (2013) with the model reported by Ma (2015). The V_p/V_s ratio is assumed to be constant at 1.74.

5. Aftershock Relocation

In this section, the aftershock relocation results are provided, and the following are presented: (1) the location process for the ME (aftershock No. 11 in Table 1), (2) the hypocentral distributions of the 68 relocated aftershocks, (3) the correction of the relocated epicenters, (4) features of the relocated hypocenters, and (5) comparisons of the obtained hypocenters to those determined by the revised-hypoDD and the International Seismological Centre (ISC).

5.1. Relocations and the residuals of the ME and its two SEs

We selected a m_N 3.5 aftershock (No. 36 in Table 1) as an ME. Its waveforms are presented in the upper three traces of Figure 6. This aftershock had very clear onsets of phases Pg and Sg at KLN, Pg at EBN, and Pn at GGN. A focal depth of 4.5 km for this aftershock was previously estimated using the depth phase sPmP, recorded at EBN, and the epicenter (47.0°N, 66.6°W) of the mainshock (Ma and Motazedian, 2017; Table 1). However, the sPmP - PmP time could not be accurately measured at EBN (see Figure 4 and Figure 5 in Ma and Motazedian, 2017), resulting in an uncertainty of about 1.0 km in focal depth. In this paper, we improved the depth estimate by using the depth phase sPg at KLN. Figure 7 demonstrates the depth phase sPg modeling for the ME. The top trace U_D/5.5 was generated using a depth of 5.5 km; other synthetic traces were generated with a depth increment of 0.1 km. The sPg - Pg time along trace U_D/5.9 and the time difference along the observed trace were approximately equal, so the modeled focal depth was 5.9 km. As the arrival times of Pg and sPg could be precisely compared, the uncertainty in the focal depth obtained by using sPg was reduced. When the onset of the depth phase sPg is clear, most of the uncertainty in the focal depth obtained by the depth phase method is proportional to the uncertainty in the velocity model (Ma and Eaton, 2011). Only the parts above and near the hypocenter are related to the travel time calculations of Pg and sPg. When we assume that the uncertainty in the crustal model is $\pm 5\%$, the uncertainty in absolute depth is about 0.3 km ($6 \times 0.5\%$).

After the focal depth for the ME was obtained, the SEISAN computer program was run again at the newly obtained focal depth value. During the first trials of the epicentral relocation, the residuals between the arrival times of the observed and the calculated Pn phases at GGN were not small, so the P wave velocity value in the crustal model beneath the Moho was adjusted to 8.25 to reduce the residuals. The epicenter and other parameters in the output file are presented in Table 2 (first row, second column). For the ME the Pg and Sg residuals at station KLN are 0.001 s and -0.001 s, respectively. The Pg residual at EBN is -0.001 s, and the Pn residual at GGN is 0.001 s. These residuals are very small. The outputs from the original computer program are ± 0.00 s. In order to observe the details of the ± 0.00 we revised the program, and ran it again to obtain ± 0.001 .

Using the same crustal model as that used for the ME, the residuals for aftershocks No. 11 and No. 44 are also not large. The residuals are listed in Table 2 (column 2; rows 2 and 3).

The precision of arrival time readings is to 2 decimal places, while the residuals of the ME (No. 36) are ± 0.001 . When these residuals are subtracted from the arrival time readings of other aftershocks, the relocated results are not affected. The reason is that the computer program takes the arrival time readings with 2 decimal places. The residuals of aftershock No. 11 are ± 0.011 or smaller. When aftershock No. 11 is treated as an alternative ME and its residuals are subtracted from arrival time readings of the other two aftershocks and itself, the relocated results change slightly or do not change. Column 3, and rows 1, 2, and 3 of Table 2 present the relocated results for aftershocks No. 36, No. 11, and No. 44 after the residual corrections were performed. The residuals of aftershock No. 11 become very small (± 0.001). Its epicentre and the origin time solutions do not change. The changed output parameter is the error at longitude; 4.1 km changes to 4.0 km. The screen output shows $RMS = 0.0$ for this aftershock. Havskov and Ottemöller (2010, page 122) stated that: “A good test of checking that residuals have been added correctly is to check the location and RMS of the master event. The RMS should be 0 and the location the same as before.” Our results match the above statement. The residuals of aftershocks No. 36 and No. 44 increased. The epicentre of No. 36 was moved from (46.977° , -66.612°) to (46.978° , -66.612°), and the epicentre of No. 44 was moved from (46.967° , -66.586°) to (46.968° , -66.586°). Both epicentres were moved northwards by about 0.1 km. The above tests show that when aftershock No. 36 is selected as an ME, residual corrections to other aftershocks are not required. We also tested that when aftershock No. 11 (the mb 5.0 principal aftershock) was used as an alternative ME, some of the epicentres of the aftershocks from No. 12 to No. 21 in Table 1 moved about 0.1 km, and some did not move. As aftershock No. 11 has an epicenter determined using the epicenters of small aftershocks detected in the second field survey (Wetmiller et al., 1984), and it produced an ignorable impact on other epicenters when it was used as an alternative ME, so it was used to perform epicenter correction in section 5.4.

5.2. Relocation of the 68 aftershocks that have records at KLN, EBN, and GGN

The aftershocks with $m_N \geq 2.8$ that occurred in 8 years after KLN was installed usually had clear onsets of Pg and Sg phases recorded at KLN, Pg at EBN, and Pn at GGN. Of the 113 aftershocks for which the focal depths were determined using a depth phase modeling procedure (Ma and Motazedian, 2017), 68 satisfied the requirements for using the ME relocation method; i.e., they had the same phase records at the same stations. Therefore, 68 aftershocks were relocated at the focal depths determined using sPg. The epicenters of the 68 aftershocks are listed in Table 1 and plotted in Figure 8 (a).

Arrival time readings for the ME (Table 2) and all the SEs were precise to 2 decimal places, and as the ME phase residuals were very small (Table 2), there was no need to apply station corrections for the 67 SEs.

5.3. Error estimates in the relative locations of epicenters

When the azimuthal coverage of an event is not good, the calculated location can move away from the true location because of the inaccuracy in the velocity model (Lienert and Havskov, 1995). Figure 1 (a) shows that station coverage was not good, and epicentral shifts were unavoidable in the epicenters we obtained. In this section, we examine the uncertainties (errors) in the relative locations between one epicenter and another. If the errors are small, the patterns of the epicentral distribution are reliable.

Errors in locations could be caused by inaccuracies in the crustal model. To examine if the errors in the relative locations of two epicenters in a group were small, a relocation test for the ME and one SE was performed. We chose two aftershocks (the ME, No. 36, and an SE, No. 44, in Table 1; both have clear onsets) and applied different crustal models given in Figure 5 and different crustal thicknesses. Figure 9 shows the obtained epicenters of the two aftershocks using the same two data sets of arrival time readings but different crustal models and crustal thicknesses. The solid circle with mb 5.7 in Figure 9 shows the location of the mainshock, determined by Wetmiller et al. (1984); the two solid squares show the locations of the ME and SE, obtained using our crustal model (Figure 5; thick lines) and a crustal thickness of 32 km. The two solid circles labeled 32, 34, 36, and 38 mark the epicenters of the same two aftershocks obtained using the GSC crustal model (Figure 5; dashed lines) and crustal thicknesses of 32, 34, 36, and 38 km, respectively.

As shown in Figure 9, the epicenters of the two aftershocks mainly shifted southwards, and the relative locations of the two aftershocks were visually unchanged because the absolute locations were determined using the calculated travel times, the same crustal model, and the same two sets of observed arrival times. When the parameters in the crustal model change, an increase or decrease in the calculated travel times causes the epicenter to move accordingly. Because the relative locations are mainly determined by the differences in the two sets of observed travel times (Figure 6), they were unchanged. Therefore, this test shows that the errors in the relative locations in a group, caused by errors in the crustal model, are very small. In other words, errors in a crustal model cause systematic errors in the epicenters of an earthquake group.

Qualitatively speaking, two major types of errors, errors in the crustal model and in the phase arrival time readings, cause the errors in the epicenters. The errors in the epicenters caused by arrival time reading errors may be roughly estimated. Along the top trace in Figure 6, the Sg - Pg time is $\delta t = 6.97 - 4.00 = 2.97$ s. If the P-wave traveled to station KLN with $V_p = 6.2$ km/s, and $V_p/V_s = 1.74$, the distance between the station and the epicenter is $r = \delta t \times V_p / (1.74 - 1) = 24.88$ km. Because the precision of arrival time readings is to 2 decimal places (Figure 6), the reading error in t is ± 0.02 s, and the error in the station distance is $\delta r = 0.02 \Delta = \pm 0.02 \times V_p / (1.74 - 1) = \pm 0.17$ km. This error could have a different sign for different aftershocks. In addition, if the error in the crustal model causes a +3.5 km error in the latitude of an aftershock, the total error (error in the crustal model and the error in arrival

time readings) is $+3.5 \pm 0.17 = +3.67$ or $+3.33$ km.

Because the same crustal model and arrival time readings of the same four phases at the same three stations were used to relocate the aftershocks, the signs for the absolute errors in the output files should be consistent. For example, the epicenter of aftershock *a* is $(46.977^\circ \pm 3.2\text{km}, -66.612 \pm 3.1\text{km}; \#36$ in Table 1), and the epicenter of aftershock *b* is $(46.982^\circ \pm 3.3\text{km}, -66.613 \pm 3.2\text{km}; \#37$ in Table 1). For aftershock *a*, if we take $(46.977^\circ + 3.2\text{km}, -66.612 - 3.1\text{km})$, then *b* is $(46.982^\circ + 3.3\text{km}, -66.613 - 3.2\text{km})$. In other words, for all aftershocks, the same sign of the errors (+ or -) needs to be assigned because the same crustal model and the same number of the arrival time readings were used to relocate the aftershocks in a group. The error caused by the crustal model dominates the total error in an epicenter in the output files of the location computer program.

The errors in the relative locations of two adjacent aftershocks may be mathematically estimated using the absolute errors in their epicenters. Assume that the epicenters of any two adjacent earthquakes *a* and *b* are (latitude_a, longitude_a) with errors (err_na, err_ea) and (latitude_b, longitude_b) with errors (err_nb, err_eb). If vectors $\mathbf{A} = \mathbf{A}_0 + \mathbf{A} = (\text{latitude_a}, \text{longitude_a}) + (\text{err_na}, \text{err_ea})$ and $\mathbf{B} = \mathbf{B}_0 + \mathbf{B} = (\text{latitude_b}, \text{longitude_b}) + (\text{err_nb}, \text{err_eb})$, then the vector difference is $\mathbf{C} = \mathbf{B} - \mathbf{A} = (\mathbf{B}_0 - \mathbf{A}_0) + (\mathbf{B} - \mathbf{A}) = \mathbf{C}_0 + \mathbf{C}$. We then obtain $\mathbf{C}_0 = (\text{latitude_b} - \text{latitude_a}, \text{longitude_b} - \text{longitude_a})$ and $\mathbf{C} = (\text{err_nb} - \text{err_na}, \text{err_eb} - \text{err_ea})$. Vector \mathbf{C}_0 shows the location of *b* relative to *a*, while vector \mathbf{C} shows the errors in the location of *b* relative to *a*. Assume aftershock No. 8 in Table 1 is *a* and one of its adjacent aftershocks, No. 14, is *b* [Figure 8 (a)], the errors in the location of No.14 relative to that of No.8 are -0.1 km (2.5 - 2.6) in latitude and -0.1 km (1.8 -1.9) in longitude. No. 13 and No. 15 are adjacent, and the errors in their relative location are (-0.1 km, -0.1 km).

For any given aftershock in Table 1, its neighbor events can be found by comparing its distances to any other aftershock. For a given aftershock the distance from its closest neighbor event, the module of its \mathbf{C} with its closest neighbor, and the ratio of this module over this distance are listed in Table 1. The average of the modules is 0.183km, which is much smaller than the gap indicated by the line with an arrow at Az 38° in Figure 8(a) or that indicated by the vertical line in Figure 11 (a); as a result, the pattern obtained hypocenters is reliable.

The distance between the epicenter of the aftershock mb 5.0 obtained by Wetmiller et al. (1984) and the epicentre we obtained for the same aftershock is 3.5 km [Figure 8 (a)], which means that all the epicenters we obtained moved about 3.5 km southwards. Because the P- and S-phases were used at a portable network (stations near the seismic activity area were less than about 10 km away) to detect small aftershocks, the epicenter of the mb 5.0 obtained by Wetmiller et al. (1984) is more reliable. This is partly because early aftershocks were located (thus more likely to be close to the rupture); and readings from close-by field stations were used; the pattern of aftershocks was compact. Therefore, we corrected our epicenters based on their epicenter of the mb 5.0.

5.4. Epicenter corrections

As the station coverage was poor, the available arrival time readings were very limited, and a 1-D crustal velocity model used in the SEISAN program, an epicentral shift relative to its true location was unavoidable. To obtain an epicentral distribution with absolute errors as small as possible, we performed an epicentral shift correction.

The star labelled S2 in Figure 8(a) marks the location of the mb 5.0 principal aftershock. This location was the centre of the small aftershocks, detected by Wetmiller et al. (1984). The solid circle labelled mb 5.0 to the southeast of the star indicates the location we determined for the same aftershock. The location was shifted southeast by about 3.5 km from the location determined by Wetmiller et al. (1984). The shift was caused by many factors, and the main one was that only a 1-D velocity model was used in the SEISAN program.

To obtain a distribution of epicenters with possibly small absolute position errors, we corrected the epicenters in Table 1. The epicenter of the mb 5.0 aftershock determined by Wetmiller et al. (1984) was assumed to have smaller absolute errors compared to the value we obtained because Wetmiller et al. (1984) used the arrival times at portable stations. As those stations were close to the seismic activity area (the stations were less than 10 km away), the absolute errors in the small aftershocks they detected were small. Accordingly, the absolute errors in the epicenter of the mb 5.0 they obtained using the center of the small aftershocks were smaller than those we obtained. The difference between S2 (latitude and longitude) and the epicenter we obtained for the mb 5.0 earthquake was subtracted from the epicenters of all 68 aftershocks in Table 1. Figure 1(b) shows the epicentral shift-corrected distribution.

5.5. Features of the relocated hypocenters

After the epicenter shift correction, the mainshock is located within the southern part of the relocated aftershock cluster [Figure 1 (b)]. As shown in Figure 8 (a), most aftershocks occurred within a 5×5 km area, with the remaining ones scattering to the southwest. Overall, the aftershocks trend in a northeasterly direction (about 038°) that is inconsistent with the topographic trend shown in Figure 1(a) and is close to the strike of one nodal for the mainshock obtained by the CMT group (202°) and by Choy et al. (1983; 195°). (see the data and resources section). Within the overall trend, the relocated aftershocks close to the mainshock appear to form a pair of northeast trends separated by a gap region indicated by a dashed-line at 038° .

To observe more distribution features of the 68 relocated hypocenters, we projected the hypocenters onto two vertical planes. The two directions are shown in Figure 8(a). Figure 10 (a) shows the projection along 038° . From Figure 10, we found that most aftershocks occurred above the mainshock in a depth range of 2 to 6 km. Figure 11(a) shows the projection along 128° . The gap region indicated by a vertical dashed line in the figure separates the aftershocks into two groups. The hypocenters on the left side of the vertical line were clustered

together, and most were in a depth range of 4 to 6 km, a narrower depth range than to the right. The projections of these hypocenters onto the surface are the epicenters on the upper-left side of the 38° line in Figure 8 (a).

5.6. Comparing the relocated epicenters with those obtained using the revised-hypoDD

Two methods are used in the hypoDD program package to solve the DD equations (Waldhauser and Ellsworth, 2000). The singular value decomposition (SVD) method is used to solve small systems. When the system to be solved becomes larger, SVD is inefficient, and therefore, the conjugate gradient algorithm LSQR (Sparse Linear Equations and Least Square) of Paige and Saunders (1982) is used to find the solution. In the Miramichi sequence, only 68 aftershocks are to be relocated; the SVD method should be able to solve the DD equations. After several tests were performed using the SVD method, we found that when the same data set was used, the solutions were not stable. One case is that a 64-bit computer can obtain solutions normally, but a 32-bit computer cannot. We performed several tests using the LSQR method and the solutions were stable. The epicenters obtained in one test are plotted in Figure 8 (b). The data set of the Pg and Sg arrival time readings for the master-event method were used, and the epicenters in Figure 8 (a) were the initial input. Of the 68 aftershocks, 64 obtained solutions. Comparing Figure 8 (b) with (a), we found that the basic pattern the epicenters formed are similar.

To facilitate comparisons, we corrected the epicenters using the same procedure described in the *Epicenter correction* section and projected the 64 hypocenters onto vertical planes at azimuth 38° and 128° . Figure 10 (b) shows the projections along a vertical plane at 38° . The basic patterns are similar to those in panel (a). Figure 11 (b) shows the projections along a vertical plane at 128° . The basic patterns are also similar to those in Figure 11 (a). In Figure 11 (a) and (b), the majority of the aftershocks project into an area about 5 km wide by 5 km deep.

5.7. Comparing the relocated hypocenters with those by ISC

We downloaded the catalogue, from the IRIS database, determined by the International Seismological Centre (ISC), of the Miramichi aftershocks that occurred in the same time period as those listed in Table 1 for comparison. Table 3 lists the downloaded catalogue. To compare the epicentral distributions, we plotted the epicenters from Table 3 in Figure 12(a) and the 68 shift-corrected epicenters in Figure 12(b). The star labeled S1 marks the epicenter of the mainshock. In (a) the mainshock is on the southeast side, while in (b) it is located within the relocated epicenter group. Both (a) and (b) roughly show linear trends in a northeasterly direction, which may indicate the strike direction of the major activated fault on which the mainshock occurred. In (a) the distribution is scattered over a larger area (about 7×15 km), while the distribution in (b) shows that most aftershocks are distributed over an about 5×5 km area. In (b), the aftershocks within the dashed oval may indicate the stress adjustment near the

source region of the mainshock.

Figure 13(a) shows the depth distribution of the ISC catalogue, prepared using the depth values in column H in Table 3. Of the 54 ISC aftershocks, 17 were listed at a nominal depth of 5 km. The remaining aftershocks were more broadly distributed than our catalogue, extending from the surface to a depth of about 15 km. This result is understandable because we expect focal depth uncertainty to be greater in the ISC catalogue possibly due to their use of P- and S-wave arrivals at teleseismic stations. Figure 13(b) shows the depth distribution of our relocated aftershocks. Most aftershocks occurred in a depth range of 2 km to 6 km. The greater uncertainty in (b) results mainly from lower shaking frequencies being better retained at teleseismic distances leading to a larger uncertainty in the arrival time readings.

6. Discussion and conclusion

Forty years ago, on 9 January 1982 in the Miramichi region of north-central New Brunswick, an earthquake with magnitude m_b 5.7 [newly determined M_W 5.6; Bent, 2015] occurred. At that time, digital seismographs had not been widely deployed, and its source parameters were not well determined. We analyzed the aftershock seismograms and found that at station KLN, there were very clear onsets of Pg- and Sg-waves, at EBN, there were clear onsets of Pg-waves, and at GGN, there were clear onsets of Pn phase for the larger aftershocks. We also unexpectedly found that the depth phase sPg was well developed and recorded at station KLN. Once the velocity records were converted into displacement records, the onsets of the depth phase could be read correctly and accurately. The depth phase information can be used to determine focal depth accurately, and the Pg, Sg, and Pn arrival time readings at the three stations can be used to determine epicenters and the origin times using a conventional location method. To obtain a reliable epicentral distribution pattern, the uncertainties (errors) in the relative locations of the epicenters need to be small. To reduce errors in the relative locations, we used a master-event method; specifically, we used the elite part in the master-event method. There were several steps to determine source parameters (epicenter, origin time, and depth) for an aftershock: (1) chose waveform records with clear onsets of Pg and Sg at stations KLN, Pg at EBN, and Pn at GGN; (2) converted the KLN velocity record into a displacement record to find a clear depth phase sPg, so determining the focal depth using a depth phase modeling method; (3) located an epicenter using a conventional location method at the determined focal depth. By using arrival time readings of the same four phases at the same three stations, the errors in the relative locations of adjacent aftershocks were shown to be small.

In our study on the relocation of the larger aftershocks in the Miramichi sequence, we attempted to reduce the errors in the relative hypocenters. The errors in the relative depths of two adjacent aftershocks were on the order of 0.1 km, which was the depth increment used to generate the synthetic seismograms. The errors in the relative locations between an epicenter and its closest neighbor events are listed in Table 1. Most of the numbers in the modu column

are less than or equal to 0.3 km, which is smaller than the narrowest part of the gap indicated by the dashed vertical line in Figure 11 (a). In another word if any epicenter in the left group is moved 0.3 in any direction, it cannot go into the right group. The two groups phenomenon remains. The above information indicates that the pattern of two groups is reliable.

Following the Miramichi mainshock, the USGS deployed a portable digital seismograph network (Cranswick et al., 1982). The 40 epicenters they located from 15 to 22 January and the network are plotted in Figure 12 (c). Comparing (c) with (b), we found that the 40 aftershocks were distributed in the same region as our final epicenters.

The largest aftershock in the first survey by Wetmiller et al. (1984) is m_N 2.8 at (47.003°N; 66.619°W), indicated with a small square labelled W in Figure 12 (b). Saikia and Herrmann (1985) relocated four aftershocks out of the 40 aftershocks determined by the USGS. These aftershocks are indicated by four diamonds in Figure 12 (b). Both the m_N 2.8 aftershock located by Wetmiller et al. (1984) and the 4 aftershocks by Saikia and Herrmann (1985), and the other 36 USGS-located aftershocks should have small epicenter errors because local records from within about 10 km of the seismic activity area were used (Fig. 10 in Wetmiller et al., 1984; Figure 12 (c) in this paper). The above aftershocks and the final epicenters we located are in the same region. Because the aftershocks that were located by Wetmiller et al. (1984), Saikia and Herrmann (1985), and the USGS, and the aftershocks we relocated are in the same earthquake sequence, the epicenters we obtained are reasonable.

In 1982, available digital seismic stations were sparse, and therefore, their coverage may not satisfy the requirements of modern technique hypoDD. The hypoDD manual states that “If P- and S-wave data is used, the threshold has to be higher to actually reach 8 stations per event pair” (Waldhauser, 2001). Consequently, the threshold must be 6 stations for the revised-hypoDD because there are 6 unknown parameters to be solved per event pair (the two fewer representing the 2 independently determined depths). For an event, the number of equations that can be formed is determined by its assigned number of neighbors, event separation distance, and the available P- and S-wave readings. In the Miramichi sequence, there are 4 readings for each event. When 3 events are in a cluster within the assigned separation distance, the first event can form 4 equations with the second and 4 equations with the third, and the second event can form 4 equations with the third. The total number of equations is 12, while there are 9 unknown parameters (3 parameters per event) to be solved. In other words, if 3 or more aftershocks are in a cluster in the Miramichi sequence, they can be resolved using the revised-hypoDD. Recently, we started another study on the revised-hypoDD, and we will introduce more results in the future. (*The results from the revised-hypoDD support what we obtained using the master-event method, but did not provide extra useful information to the readers. In fact, each hypocenter solution is related to arrival time readings of other events along a chain. The solutions of the events along a chain come from trade-off when*

the computer solves the equations formed by the arrival time readings of those events a long a chain. Logically the solutions provided in this article are not better than those obtained using the master-event method, in which no trade-off between events exists. The only connection is the crustal model commonly used. All the parts related to the revised-hypoDD could be removed from this article).

Crustal velocity models provide fundamental information, but good models for a region are hard to obtain. As all aftershocks are shallower than 10 km, the first and second layers in Figure 5 are used to calculate the travel times of P- and S-phases at stations KLN and EBN. To reduce the Pn-phase residuals at GGN, we slightly adjusted the Moho depth and the P-wave velocity beneath Moho when the ME was relocated. Unfortunately, we do not have an optimal crustal model between the Miramichi earthquake source region and the path to station GGN available at this time.

The aftershocks we relocated were in 8 years when KLN station was operated. Since the mainshock occurrence 40 years past, the aftershock activity in the source region still continues. The mystery related to the Miramichi earthquake sequence, such as why there are so many aftershocks, and several principal aftershocks followed the mainshock, is still waiting for people to explore.

Based on the analyses of the relocated aftershocks in the previous sections, the following can be concluded: (i) the major source volume was about $5 \times 5 \times 5$ km³, (ii) the focal depths ranged from about 2 km to 6 km, (iii) two major rupture regions were activated; one was caused by the mainshock and the other one possibly by the mb 5.4 principal aftershock, and (iv) the trends in the aftershock epicenters were close to the northeast strike of the nodal plane for the mainshock. Lastly, the trends were also consistent with the topographic trend near the source region.

Data and Resources

The seismograms used in this study were collected from the Natural Resources Canada (NRCAN) at <http://www.earthquakescanada.nrcan.gc.ca> (last accessed in November 2016). The *SEISAN program tutorial* by Havskov, Ottemöller, and Voss (2014) was downloaded from <http://seisan.info/seisan-tutorial.pdf>. The Global CMT Catalog is available at <http://www.globalcmt.org/CMTsearch.html>.

Acknowledgements

This research was supported by the Natural Sciences and Engineering Research Council of Canada under the Discovery Grant program. We gratefully acknowledge the constructive comments, suggestions, and text revisions from Dr. John Adams at Natural Resources Canada, and the reviewers *** ***, and the Editor ***. The waveform records were processed using SAC, *redseed*, and *geotool* programs. The location program *HYPOCENTER* in the SEISAN program package was used; Figure 1 was prepared using the software GMT (Wessel and Smith, 1991).

References

- Basham, P. W. and J. Adams (1984), The Miramichi, New Brunswick Earthquakes: Near-surface thrust faulting in the Northern Appalachians, *Geoscience Canada*, 11(3), 115-121.
- Bent, A. L. (2009), A moment magnitude catalog for the 150 largest eastern Canadian earthquakes. Geological Survey of Canada, Open File 6080, 2009; 23 pages, doi:10.4095/247618
- Bouchaala, F., V. Vavryčuk, and T. J. Fischer (2013), Accuracy of the master-event and double-difference locations: synthetic tests and application to seismicity in West Bohemia, Czech Republic, *Journal of Seismology*, 17(3), 841–859.
- Choy, G. L., J. Boatwright, J. W. Dewey, and S. A. Sipkin (1983), A teleseismic analysis of the New Brunswick Earthquake of January 9, 1982, *J. Geophys. Res.*, 88, 2199–2212. doi:10.1029/JB088iB03p02199.
- Cranswick, E., C. Mueller, R. Wetmiller, and E. Sembera (1982), Local Multi-Station Digital Recordings of Aftershocks of the January 9th, 1982 New Brunswick Earthquake, USGS, Open-File Report 82-777.
- Frémont, M.J. & S. D. Malone (1987), High precision relative locations of earthquakes at Mount St. Helens, Washington, *J. Geophys. Res.*, 92(B10), 10223–10236.
- Havskov, J. and L. Ottemöller (1999), SEISAN Earthquake Analysis Software, *Seismol. Res. Lett.* 70, 5.
- Havskov, J. and L. Ottemöller (2010), Routine Data Processing in Earthquake Seismology, with Sample Data, Exercises and Software. DOI 10.1007/978-90-481-8697-6, 347 pp, Springer Dordrecht Heidelberg London, New York.
- Halchuk, S., Allen, T.I. Allen, G. C. Rogers, and J. Adams (2015), Seismic Hazard Earthquake Epicentre File (SHEEF2010) used in the Fifth Generation Seismic Hazard Maps of Canada; Geological Survey of Canada, Open File 7724. 1 .zip file. doi:10.4095/296908.
- Klein, F. W. (2002), User's Guide to HYPOINVERSE-2000, a Fortran Program to Solve for Earthquake Locations and Magnitudes. U. S. Geological Survey, Open File Report 02-171.
- Langston, C. (1987), Depth of faulting during the 1968 Meckering, Australia, earthquake sequence determined from waveform analysis of local seismograms, *J. Geophys. Res.*, 92(11), 561–11,574.
- Lienert, B. R. E., E. Berg, and L. N. Frazer (1986), Hypocenter: An earthquake location method using centered, scaled, and adaptively least squares, *Bull. Seismol. Soc. Am.* 76, 771-783.

- Lienert, B. R. E. (1991), Report on modifications made to hypocenter. Technical report, Institute of Solid Earth Physics, University of Bergen, Bergen, Norway.
- Lienert, B. R. E. and J. Havskov (1995), A computer program for locating earthquakes both locally and globally, *Seismol. Res. Lett.* **66**, 26-36.
- Ma, S. and G. M. Atkinson (2006), Focal depth distribution for earthquakes with $m_N \geq 2.8$ in western Quebec, southern Ontario and northern New York, *Bull. Seismol. Soc. Am.* **96**, 609–623.
- Ma, S. (2010), Focal depth determination for Moderate and Small Earthquakes by Modeling Regional Depth Phases sPg, sPmP, and sPn, *Bull. Seismol. Soc. Am.* **100**, 1073–1088.
- Ma, S. and D. Eaton (2011), Combining double-difference relocation with regional depth-phase modelling to improve hypocentre accuracy, *Geophys. J. Int.* **185**, 871–889. doi: 10.1111/j.1365-246X.2011.04972.
- Ma, S. (2015), S-wave velocity models obtained using Rg wave dispersion data at shallow parts of the crust in the southern New Brunswick region. Report to: Natural Resources Canada, Ottawa, ON, Canada (contract No. 3000565835).
- Ma, S. and D. Eaton (2011), Combining double-difference relocation with regional depth-phase modelling to improve hypocentre accuracy, *Geophys. J. Int.*, **185**(2), 871–889, doi: 10.1111/j.1365-246X.2011.04972.x
- Ma, S. and D. Motazedian (2012), Studies on the June 23, 2010 north Ottawa M_W 5.2 earthquake and vicinity seismicity, *Journal of Seismology*, **16**, 513–534. doi: 10.1007/s10950-012-9294-7.
- Ma, S. and D. Motazedian (2017), Focal depth distribution of the 1982 Miramichi earthquake sequence determined by modelling depth phases, *Can. J. Earth Sci.* **54**, 359–369.
- Motazedian, D., S. Ma, and S. Crane (2014), Crustal shear-wave velocity models obtained from *Rayleigh* wave dispersion data in North-Eastern America, *Bull. Seismol. Soc. Am.* **104**(4), doi: 10.1785/0120130265.
- Nuttli, O. W. (1973), Seismic wave attenuation and magnitude relations for eastern North America, *J. Geophys. Res.* **78**, 876–885. doi: 10.1029/JB078i005p00876.
- Paige, C.C. and M.A. Saunders (1982), LSQR: Sparse linear equations and least squares problems, *ACM Trans. Math. Softw.*, **8**(2), 195–209.
- Randall, G. (1994), Efficient calculation of complete differential seismograms for laterally homogeneous earth models, *Geophys. J. Int.* **118**, 245–254.
- Saikia, C. K. and R. B. Herrmann (1985), Application of waveform modeling to determine focal mechanisms of four 1982 Miramichi aftershocks, *Bull. Seismol. Soc. Am.* **75**(4), 1021–1040.

- Stoddard P. R. and Woods M. T. (1990), Master event relocation of Gorda Block earthquakes—implications for deformation, *Geophys Res. Lett.* 17(7), 961–964.
- Uski, M., T. Hyvonen, A. Korja, and M. Airo (2003), Focal mechanisms of three earthquakes in Finland and their relation to surface faults, *Tectonophysics*, 363,141–157.
- Wessel, P. and W. H. F. Smith (1991), Free software helps map and display data. *EOS Earth and Space Science News*, 72,441–444. doi:10.1029/90EO00319.
- Wetmiller, R. J., J. Adams, F. M. Anglin, H. S. Hasegawa, and A. E. Stevens (1984), Aftershock sequence of the 1982 Miramichi, New Brunswick, earthquake, *Bull. Seismol. Soc. Am.* 74, 621-653.
- Waldhauser, F. (2001), HYPODD—A program to compute double-difference hypocenter locations, Open-File Rep. 01–113, U.S. Geol. Surv.
- Waldhauser, F. and Ellsworth, W. L. (2000), A double-difference earthquake location algorithm: method and application to the northern Hayward fault, California, *Bull. seismol. Soc. Am.*, 90 (6),1353–1368.
- Zollo, A., R. De Matteis, P. Capuano, F. Ferulano, and G. Iannaccone(1995), Constraints on the shallow crustal model of the Northern Apennines (Italy) from the analysis of microearthquake seismic records, *Geophys J. Int.* 120, 646–662.

Dariush Motazedian

Department of Earth Sciences, Carleton University

1125 Colonel By Drive

Ottawa, Ontario, K1S 5B6, Canada

Shutian Ma

Department of Earth Sciences, Carleton University

1125 Colonel By Drive

Ottawa, Ontario, K1S 5B6, Canada

Table 1. Catalogue of the relocated aftershocks for the Miramichi earthquake sequence

No date time lat. long. H m_N er_n er_e dis modu perc
(°) (°) km km km km km

1982 02 24 0443 01.0 46.977 -66.623 3.1 2.9 3.3 3.0 0.135 0.100 74
2 1982 02 27 1734 57.6 47.033 -66.566 5.6 3.4 4.2 5.8 1.732 0.608 35
3 1982 03 01 0933 57.1 46.955 -66.607 4.8 3.4 3.0 2.7 0.451 0.000 00
4 1982 03 03 00 28 32.7 46.996 -66.602 5.7 2.8 3.7 3.8 0.648 0.283 44
5 1982 03 04 0606 31.1 47.019 -66.576 5.5 2.9 4.3 5.2 1.482 1.000 67
6 1982 03 13 1138 13.0 46.995 -66.616 5.0 2.9 3.5 3.5 0.470 0.100 21
7 1982 03 13 2327 51.6 46.974 -66.545 2.8 2.9 3.8 4.3 1.408 0.224 16
8 1982 03 16 1114 01.8 46.919 -66.620 3.8 3.5 2.6 1.9 0.811 0.141 17
9 1982 03 26 0536 39.6 46.988 -66.553 5.4 2.8 3.7 4.5 1.212 0.400 33
10 1982 03 26 1338 07.3 47.006 -66.590 5.3 2.9 3.9 4.3 0.254 0.200 79
11 1982 03 31 21 02 21.2 46.979 -66.562 3.1 5.0 3.7 4.1 0.254 0.100 39
12 1982 03 31 2129 19.3 46.971 -66.575 2.8 2.9 3.5 3.5 0.254 0.141 56
13 1982 04 02 1350 12.3 46.977 -66.567 3.5 4.3 3.6 3.9 0.367 0.141 39
14 1982 04 02 1949 35.4 46.912 -66.623 3.1 3.1 2.5 1.8 2.272 0.283 12
15 1982 04 08 0454 33.9 46.980 -66.565 3.7 3.4 3.7 4.0 0.367 0.141 39
16 1982 04 11 1800 53.4 46.980 -66.615 5.7 4.0 3.3 3.1 0.076 0.000 00
17 1982 04 11 1827 19.3 46.984 -66.609 5.7 3.2 3.4 3.3 0.377 0.141 38
18 1982 04 11 2007 00.1 46.898 -66.673 5.5 2.9 2.2 1.5 0.397 0.100 25
19 1982 04 18 2247 21.3 46.958 -66.592 3.7 4.1 3.1 2.9 0.189 0.141 75
20 1982 05 02 2331 36.9 46.961 -66.616 4.3 3.3 3.1 2.8 0.793 0.141 18
21 1982 05 06 1628 07.7 46.942 -66.628 4.7 4.0 2.7 2.2 0.720 0.100 14
22 1982 06 16 11 43 30.5 47.001 -66.933 8.7 4.7 3.1 2.2 20.01 1.655 08
23 1982 06 18 1124 36.0 46.899 -66.668 4.5 3.0 2.3 1.5 1.244 0.000 00
24 1982 06 25 0647 10.3 46.931 -66.634 6.0 2.9 2.7 2.0 1.518 0.224 15
25 1982 07 18 1501 04.8 46.940 -66.619 4.6 2.9 2.8 2.2 1.518 0.224 15
26 1982 08 12 2043 18.2 46.982 -66.613 4.6 3.3 3.3 3.2 0.235 0.100 43
27 1982 09 19 0137 17.5 46.957 -66.594 6.3 3.1 3.0 2.8 0.319 0.000 00
28 1982 10 18 0437 48.9 46.967 -66.602 5.7 3.0 3.1 3.0 0.188 0.100 53
29 1982 10 21 1812 47.6 46.982 -66.617 3.9 2.8 3.3 3.2 0.222 0.000 00
30 1982 10 26 1531 33.0 46.985 -66.618 4.8 3.5 3.3 3.2 0.135 0.000 00
31 1982 10 28 0635 10.9 46.842 -66.677 5.9 2.8 2.1 1.4 1.674 0.141 08
32 1982 10 31 1244 41.4 46.999 -66.561 5.9 2.9 3.8 4.7 2.087 0.412 20
33 1982 12 22 1253 26.4 46.994 -66.610 4.8 3.0 3.5 3.6 1.114 0.316 28
34 1983 02 12 1800 25.8 46.886 -66.661 4.5 2.8 2.2 1.4 0.377 0.141 37
35 1983 05 12 2042 25.4 46.853 -66.656 3.0 3.0 2.0 1.3 1.564 0.141 09
36 1983 05 13 17 26 02.1 46.977 -66.612 5.9 3.5 3.2 3.1 0.269 0.100 37
37 1983 05 13 2340 57.4 46.982 -66.613 5.8 3.9 3.3 3.2 0.235 0.100 43
38 1983 06 10 0422 39.2 46.964 -66.626 5.9 3.3 3.0 2.6 1.202 0.361 30
39 1983 06 11 1347 58.6 46.979 -66.592 6.0 3.4 3.3 3.5 0.601 0.200 33
40 1983 06 28 0805 49.3 47.033 -66.674 2.7 3.3 3.8 3.7 6.042 0.510 08
41 1983 11 02 0602 00.4 46.857 -66.679 4.2 2.8 2.0 1.3 1.552 0.000 00
42 1983 11 17 1532 18.2 46.975 -66.614 5.6 3.7 3.2 3.0 0.470 0.100 21
43 1983 11 18 1028 39.5 46.862 -66.698 2.2 3.0 2.0 1.3 2.246 0.141 06
44 1984 02 24 03 17 13.8 46.967 -66.586 5.9 3.7 3.2 3.2 0.539 0.283 52
45 1984 03 27 2256 24.6 46.899 -66.502 3.9 3.0 2.8 2.4 9.261 0.539 06
46 1984 04 13 1535 51.3 46.974 -66.595 4.7 3.1 3.3 3.3 0.956 0.316 33
47 1984 07 02 0524 54.0 46.888 -66.665 5.9 3.0 2.3 1.5 1.918 0.224 12
48 1984 08 04 0511 13.0 46.953 -66.638 2.0 2.9 2.9 2.4 1.526 0.224 15
49 1984 10 13 0145 15.8 46.823 -66.758 2.0 3.0 1.8 1.2 3.931 0.000 00
50 1984 11 07 1944 31.5 46.959 -66.606 4.7 2.8 3.0 2.7 0.685 0.100 15
51 1984 11 30 0554 22.4 46.978 -66.622 5.0 3.8 3.2 3.0 0.470 0.100 21
52 1985 05 13 1846 19.3 46.854 -66.631 2.0 2.8 2.0 1.3 2.420 0.141 06
53 1985 10 05 0534 13.6 47.008 -66.587 6.0 3.9 3.7 4.4 0.334 0.100 30

No	date	time	lat.	long.	H	m_N	er_n	er_e	dis	modu	perc
(°)	(°)		km	km	km	km	km	km	km	km	km

The 68 aftershocks in this table match those in Figure 8 (a). Their epicenters and origin times are those outputs from computer program (no shift-correction yet); their magnitudes m_N came from the NRCan database. The magnitude type for No. 11 and No. 22 is mb. Column H lists the focal depths determined using our depth-phase modeling method. Columns er_n and er_e are the errors in km for the N-S (latitude) and E-W (longitude) directions, respectively. These error values are in the output files from the SEISAN location program (Havskov et al., 2014). dis stands for the distance between an aftershock and its closest neighbor event; modu stands for the modular of a vector formed using the errors of one aftershock and those of its closest neighbor event (section: *An error estimate in the relative locations of epicenters we obtained*); perc stands for percentage (modu/dis *100). No. 11 is indicated in Figure 8 (a); No. 22 is indicated in Figure 1(b); No. 36 and No. 44 are used in the *An error estimate in the relative locations of epicenters* section. These relocated aftershocks occurred between 24 February 1982 and 10 June 1989 when the waveform records were available at station KLN. The earthquake No. 69 is for a small aftershock, S1 for the mainshock, and S2 and S3 for the two principal aftershocks (Wetmiller et al., 1984); and the last four are small aftershocks relocated by Saikia and Herrmann (1985).

Table 2. Relocations and the residuals of the ME and its two SEs (No. 36, 11, and 44 in Table 1)

date time lat./ ^o long./ ^o	date time lat. long.
depth	depth
1983 0513 17:26 2.1	1983 0513 17:26 2.1
46.977 -66.612 5.9km	46.978 -66.612 5.9
error 0.27s 3.2km 3.1km	0.27 3.2 3.1
stat phas hhmm second	stat phas hhmm second
tres dis Az	tres dis Az
KLN P 1726 6.120. 001	KLN P 1726 6.130. 021
23.6 129	23.6 129
KLN S 1726 9.08- 0.001	KLN S 1726 9.07- 0.011
23.6 129	23.6 129
EBN P 1726	EBN P 1726
24.19- 0.001 135. 294	24.18- 0.011 135. 294
GGN Pn 1726	GGN Pn 1726
32.990. 001 207. 185	32.990. 001 207. 185
date time lat. long.	date time lat. long.
depth	depth
1982 0331 21:02 21.2	1982 0331 21:02 21.2
46.979 -66.562 3.1	46.979 -66.562 3.1
0.27 3.7 4.1	0.27 3.7 4.0
stat phas hhmm second	stat phas hhmm second
tres dis Az	tres dis Az
KLN P 2102 24.62	KLN P 2102
- 0.011 20.9 136	24.63- 0.001 20.9 136
KLN S 2102 27.22	KLN S 2102 27.210. 001
0.011 20.9 136	20.9 136
EBN P 2102 43.80	EBN P 2102
0.011 138. 293	43.790. 001 138. 293
GGN Pn 2102 52.41	GGN Pn 2102
- 0.001 208. 186	52.410. 001 208. 186

date time lat./° long./°	date time lat. long.
depth	depth
1983 0513 17:26 2.1	1983 0513 17:26 2.1
46.977 -66.612 5.9km	46.978 -66.612 5.9
error 0.27s 3.2km 3.1km	0.27 3.2 3.1
stat phas hhmm second	stat phas hhmm second
tres dis Az	tres dis Az
KLN P 1726 6.120. 001	KLN P 1726 6.130. 021
23.6 129	23.6 129
KLN S 1726 9.08- 0.001	KLN S 1726 9.07- 0.011
23.6 129	23.6 129
EBN P 1726	EBN P 1726
24.19- 0.001 135. 294	24.18- 0.011 135. 294
GGN Pn 1726	GGN Pn 1726
32.990. 001 207. 185	32.990. 001 207. 185
date time lat. long.	date time lat. long.
depth	depth
1984 0224 03:17 13.8	1984 0224 03:17 13.8
46.967 -66.586 5.9	46.968 -66.586 5.9
0.27 3.2 3.2	0.28 3.2 3.2
stat phas hhmm second	stat phas hhmm second
tres dis Az	tres dis Az
KLN P 0317	KLN P 0317
17.480. 011 21.3 130	17.490. 021 21.4 130
KLN S 0317	KLN S 0317
20.16- 0.011 21.3 130	20.15- 0.021 21.4 130
EBN P 0317	EBN P 0317
36.18- 0.001 137. 294	36.17- 0.011 137. 294
GGN Pn 0317	GGN Pn 0317
44.590. 001 206. 186	44.590. 001 206. 186

In the first column, 36, 11, and 44 are aftershock index in Table 1. The three panels in the second column show the computer outputs for aftershocks 36, 11, and 44 in Table 1. The right three panels show the computer outputs for the same three aftershocks when No. 11 was treated as an alternative master-event. tres is the residual between the observed and calculated arrival times; dis is the station distance; and Az is the station azimuth.

Table 3. ISC catalogue of the aftershocks for the Miramichi earthquake sequence

No date time lat. long. H m_N
(°) (°) km

1982 0227 1734 56 47.0397 -66.6563 10.7 3.4
3 1982 0301 0933 54 47.0507 -66.6585 7.6 3.4
8 1982 0316 1113 59 47.0241 -66.6556 4.4 3.5
1982 0318 0327 17 47.0453 -66.6761 5.0 3.2
1982 0320 0308 08 46.9975 -66.6903 0.0 3.0
11 1982 0331 2102 17 47.0619 -66.6340 2.8 5.0
13 1982 0402 1350 10 47.0620 -66.6533 12.7 4.6
14 1982 0402 1949 44 46.9795 -66.6509 5.0 3.1
15 1982 0408 0454 32 47.0118 -66.6298 13.7 3.4
16 1982 0411 1800 50 47.0649 -66.7310 5.0 4.1
17 1982 0411 1827 18 47.0077 -66.7004 8.2 3.2
19 1982 0418 2247 19 47.0105 -66.6722 10.3 4.1
1982 0428 0635 59 46.9900 -66.7268 5.0 3.4
1982 0502 0142 42 47.0118 -66.6995 6.3 3.1
20 1982 0502 2331 35 46.9818 -66.7305 8.0 3.3
21 1982 0506 1628 05 47.0772 -66.6865 7.3 4.0
1982 0616 1541 51 47.0000 -66.9500 8.0 3.0
23 1982 0618 1124 35 46.9705 -66.7220 5.0 3.0
00 1982 0728 0535 34 47.0556 -66.7689 5.0 3.7
26 1982 0812 2043 16 46.9195 -66.7508 12.6 3.3
27 1982 0919 0137 15 46.9437 -66.7002 5.0 3.1
28 1982 1018 0437 47 46.9569 -66.7039 4.6 3.0
30 1982 1026 1531 31 47.0413 -66.6828 5.2 3.5
33 1982 1222 1253 24 47.0078 -66.6839 5.0 3.0
35 1983 0512 2042 23 47.0357 -66.5600 5.0 3.0
36 1983 0513 1725 59 47.0135 -66.7061 4.7 3.5
37 1983 0513 2340 55 47.0602 -66.6631 11.1 3.9
38 1983 0610 0422 37 46.9852 -66.7398 9.0 3.3
39 1983 0611 1347 56 47.0558 -66.6075 6.4 3.4
40 1983 0628 0805 47 47.0573 -66.6828 8.0 3.3
1983 1017 2258 55 47.2105 -66.3806 5.0 3.2
1983 1116 1213 54 46.9998 -66.6369 2.4 3.2
42 1983 1117 1532 16 46.9921 -66.6357 12.1 3.7
43 1983 1118 1028 38 46.9579 -66.7234 5.0 3.0
44 1984 0224 0317 12 46.9896 -66.6473 10.7 3.7
45 1984 0327 2256 22 46.9265 -66.3928 5.0 3.0
46 1984 0413 1535 48 47.0690 -66.4878 5.0 3.1
47 1984 0702 0524 52 47.0604 -66.5586 2.7 3.0
49 1984 1013 0145 14 47.0705 -66.6174 5.0 3.0
51 1984 1130 0554 20 47.0287 -66.6831 9.6 3.8
1984 1207 2050 18 46.9159 -66.5292 12.4 3.1
53 1985 1005 0534 11 47.0236 -66.6973 5.0 3.9
54 1985 1005 0617 34 47.0000 -66.6000 5.0 3.3
55 1985 1221 0603 09 46.9878 -66.7465 5.3 3.1
56 1986 0121 0232 24 46.9495 -66.7104 9.5 3.4
1986 0306 0834 48 47.0194 -66.6172 13.2 3.4
58 1986 0601 1453 12 47.0133 -66.6781 10.8 3.4
59 1986 1017 1447 56 47.0946 -66.4949 11.3 4.1
61 1986 1023 1258 03 46.8978 -66.7377 5.0 3.4
1986 1028 1648 13 47.0244 -66.7106 14.3 3.4
63 1988 0306 1813 16 46.9929 -66.7158 9.5 3.2
64 1988 0509 0123 03 47.0365 -66.6924 10.6 3.5
66 1988 0826 0559 09 46.9659 -66.8132 6.7 3.8

No	date	time	lat.	long.	H	m_N
(°)	(°)					km

This catalogue was determined by ISC, retrieved from IRIS. These aftershocks occurred during the same time period as those in Table 1. The index numbers in column No are the same as those in Table 1. The aftershocks without an index number are not in Table 1. The total number of aftershocks in this table is 54; some aftershocks in Table 1 are not available in the IRIS database.

Figure captions

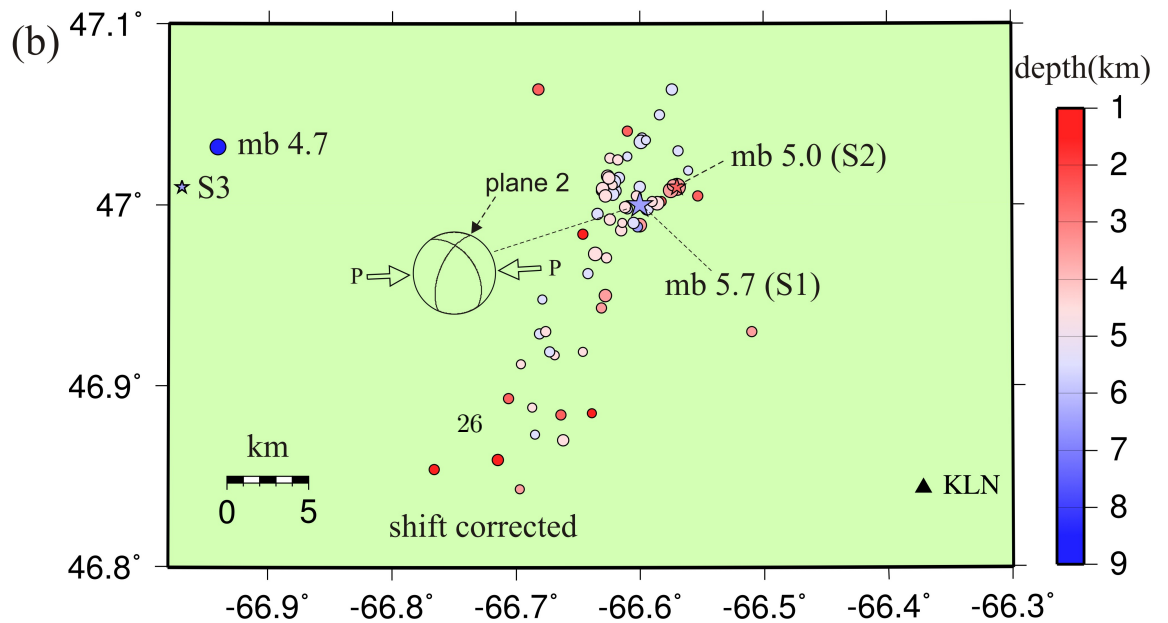
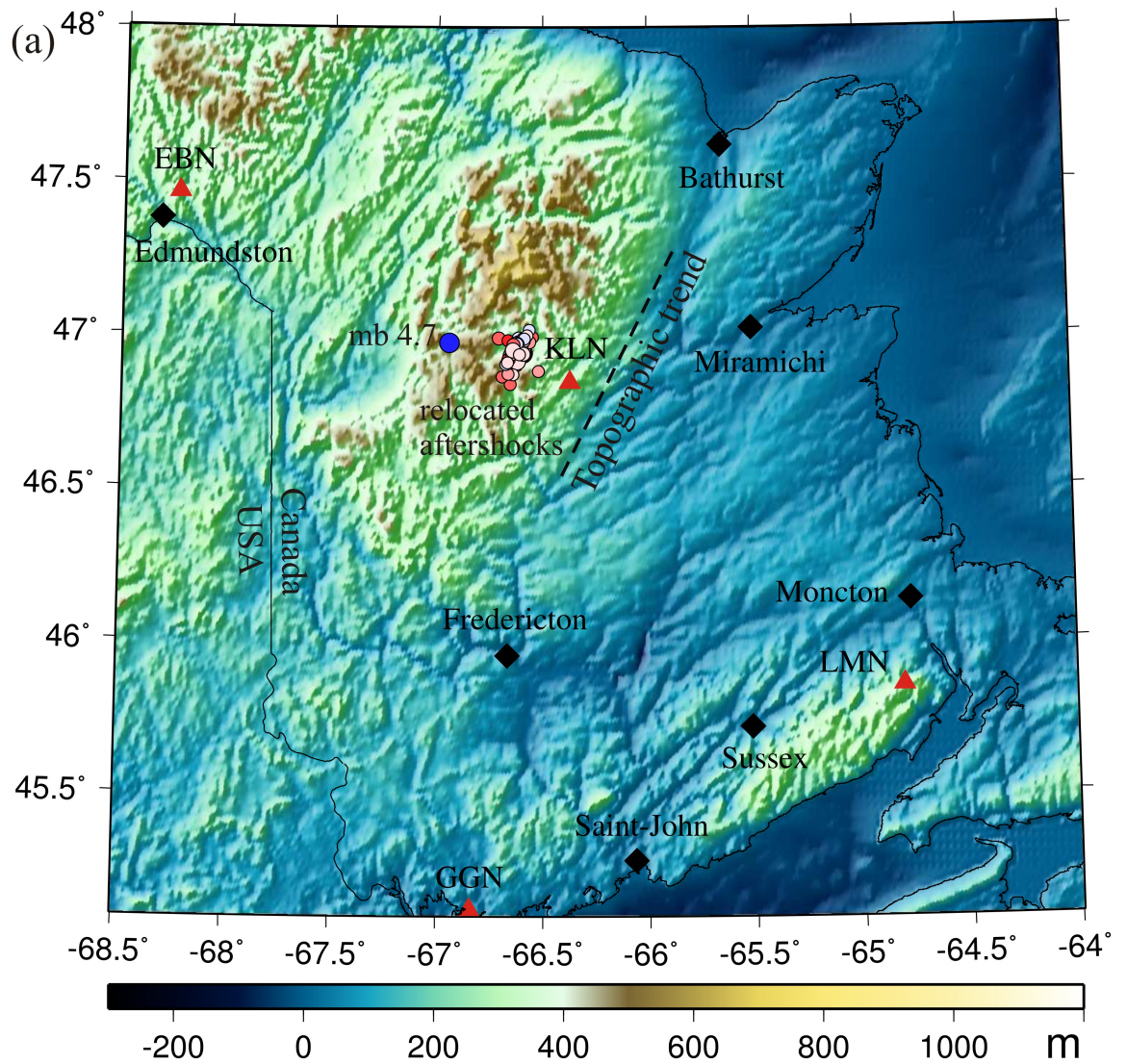


Figure 1. (a) Distributions of stations, KLN, EBN, GGN, and LMN (triangles), and the relocated aftershocks (solid circles) using a master-event method. The trend formed by the epicenters in the northeasterly direction is consistent with the topographic trend near station KLN. The diamonds represent the locations of cities or towns. (b) The enlarged epicenter zone. The color of a solid circle corresponds to a focal depth value indicated by the depth scale on the right. The approximate locations of the three field surveys and the three epicenters (Wetmiller et al., 1984) are indicated by stars, S1, S2, and S3, and the color of a star matches the focal depth. Star S2 and the solid circle for the aftershock mb 5.0 overlap. The two horizontal arrows, indicated with the letter P and pointing to the “beachball” show the compressive force directions obtained from the moment tensor solution for the mainshock (the global CMT project; globalcmt.org). The northeast trend of the epicentral distribution is consistent with the strike of the CMT’s nodal plane 2. Both (a) and (b) were plotted using the GMT program (Wessel and Smith, 1991).

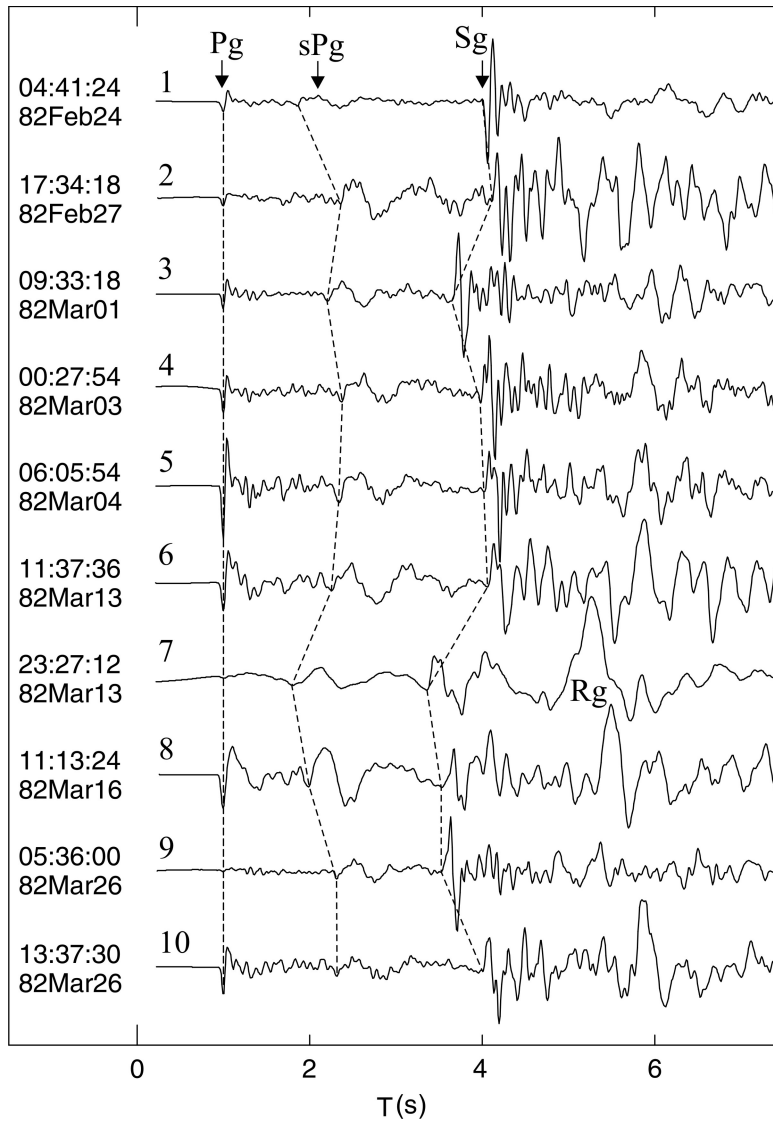


Figure 2. P-wave vertical component short period displacement seismograms recorded at station KLN, generated by the first 10 aftershocks in Table 1. All records are aligned at the Pg phase. The time on the left side of each record is the rawrecord start time. For each aftershock, the hypocentral distance to KLN is mainly constrained by the time difference $T_{Sg} - T_{Pg}$, while the focal depth is mainly constrained by $T_{sPg} - T_{Pg}$.

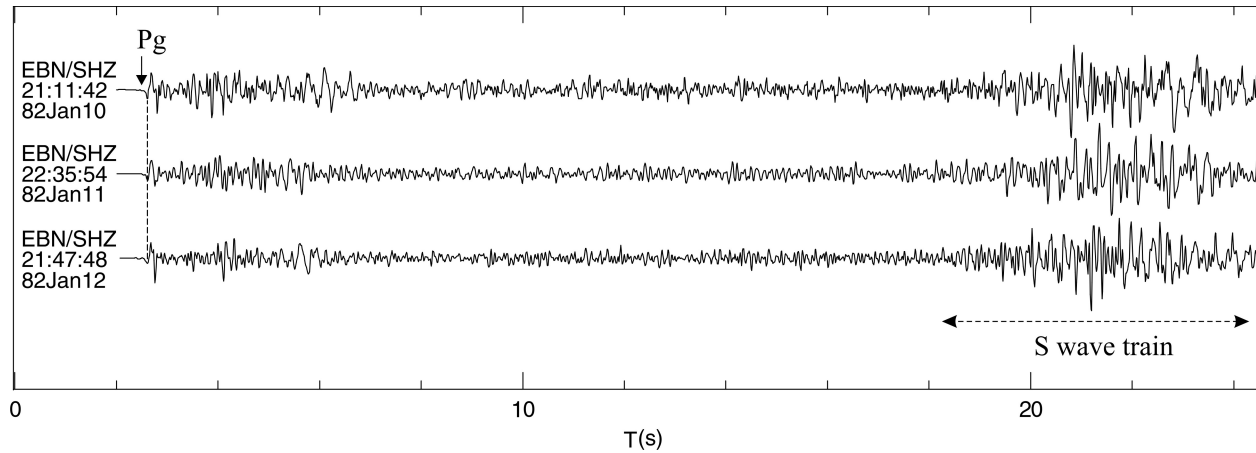


Figure 3. P-wave vertical component short period displacement seismograms recorded at station EBN (station distance ~ 135 km) generated by three aftershocks in the Miramichi sequence. On the left side of each record, the station name, channel (EBN/SHZ), and the original record start time are indicated.

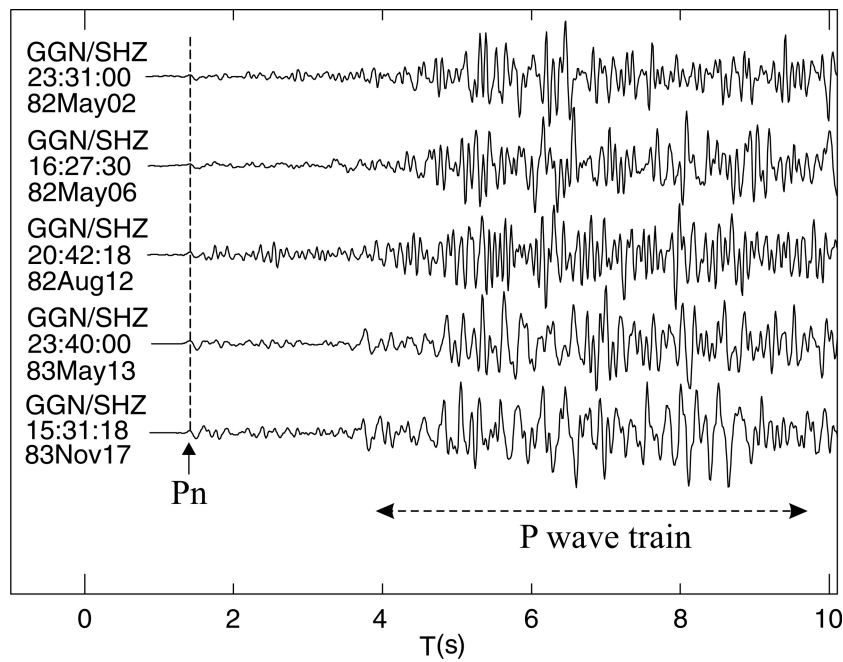


Figure 4. P-wave vertical component short period displacement seismograms at station GGN (station distance ~ 200 km) generated by five aftershocks in the Miramichi sequence. These records are aligned at the Pn phase. On the left side of each record, the station/channel names (GGN/SHZ) and the original record start time are indicated.

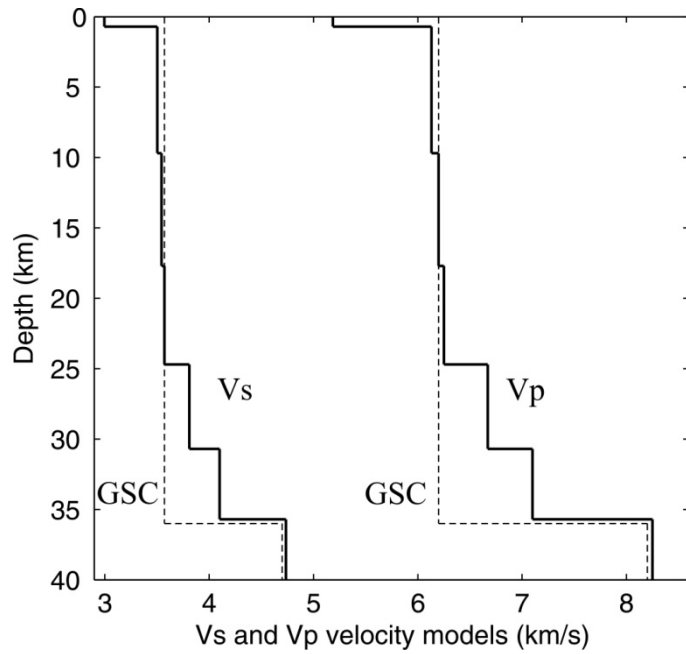


Figure 5. Crustal velocity models. The first and second layers were used to calculate the travel times of P- and S-phase at stations KLN and EBN and used to generate synthetic seismograms at KLN for the depth phase sPg modeling. The dashed lines show the crustal model used by GSC to locate events in eastern Canada, plotted here for reference.

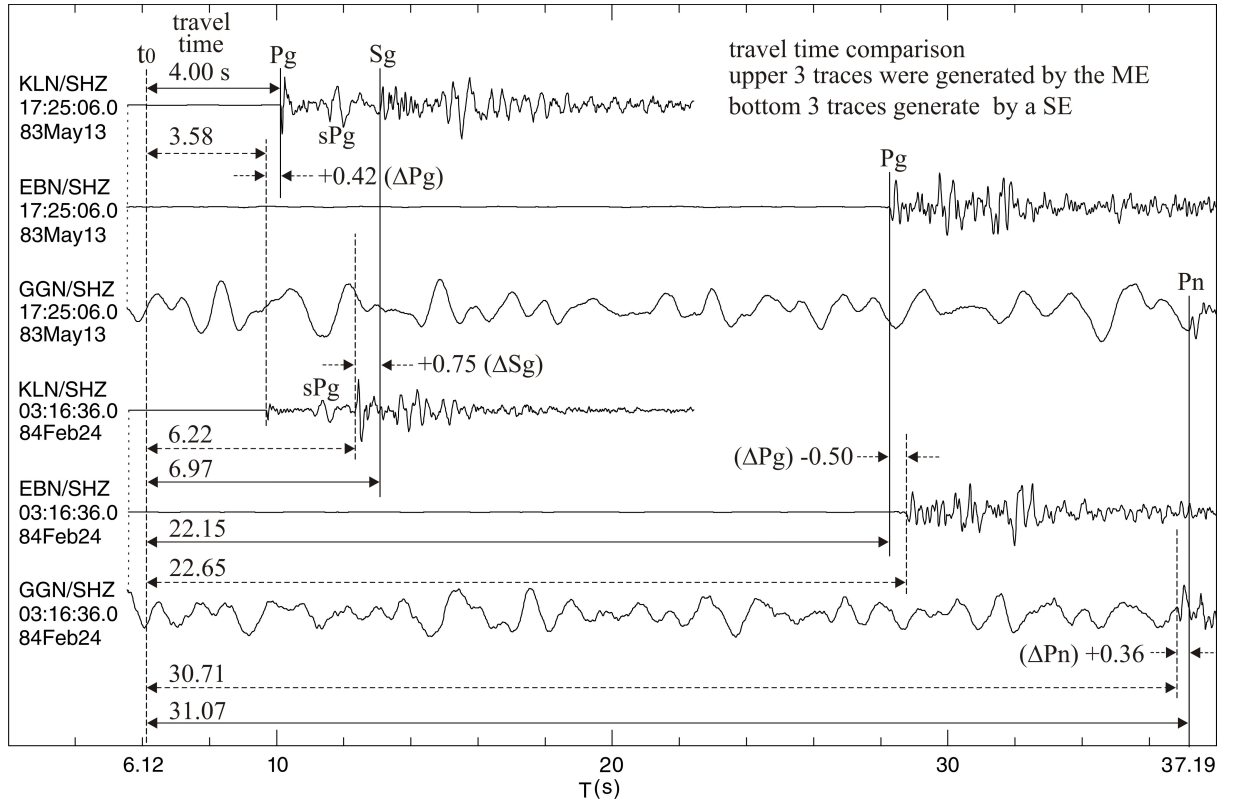


Figure 6. Travel time comparison. The upper three traces were generated by the master event (ME, No. 36 in Table 1); the bottom three traces were generated by a secondary event (SE, No. 44 in Table 1). The symbols and numbers on the left side of each trace show the station name (code), short period vertical component, and the original record start time of the trace. The time marked along the bottom axis is relative for conveniently aligning the traces. The symbol t_0 means origin time; P_g , S_g , and P_n are travel time differences. The origin times of the ME and SE were aligned for comparison (the determined values of the two origin times are in Table 1; here they are calculated using S_g and P_g arrival times). The travel times for the ME at KLN: P_g phase is 4.00 s and S_g phase is 6.97 s; at EBN: P_g is 22.15 s; at GGN: P_n is 31.07 s. The travel times for the SE at KLN: P_g phase is 3.58 s and S_g phase is 6.22 s; at EBN: P_g is 22.65 s; at GGN: P_n is 30.71 s. At KLN: P_g is +0.42 s (4.00 - 3.58) and S_g is +0.75 s (6.97 - 6.22); at EBN: P_g is -0.50 s (22.15 - 22.65); at GGN: P_n is +0.36 s (31.07 - 30.71). These differences determine the relative positions of the two aftershocks. These traces are vertically enlarged, horizontally expanded, and interpolated to 100 points/s, so the onsets are clear, and the arrival times can be measured with high precision.

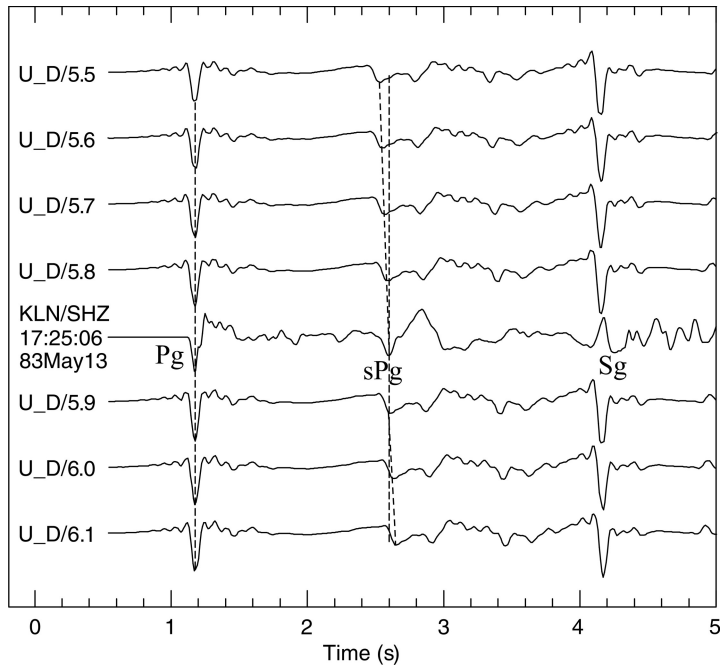


Figure 7. Regional depth phase sPg modeling at KLN (distance = 23.6 km) for the ME. The top synthetic vertical displacement trace U_D/5.5 was generated using a depth of 5.5 km. Other synthetic traces were generated with a depth increment of 0.1 km. Trace KLN/SHZ is the observed vertical short period displacement seismogram at KLN. The synthetic and the observed Pg are aligned. The time difference between sPg and Pg along trace U_D/5.9 and the time difference along the observed trace is approximately equal. Therefore, the modeled focal depth for the ME is 5.9 km.

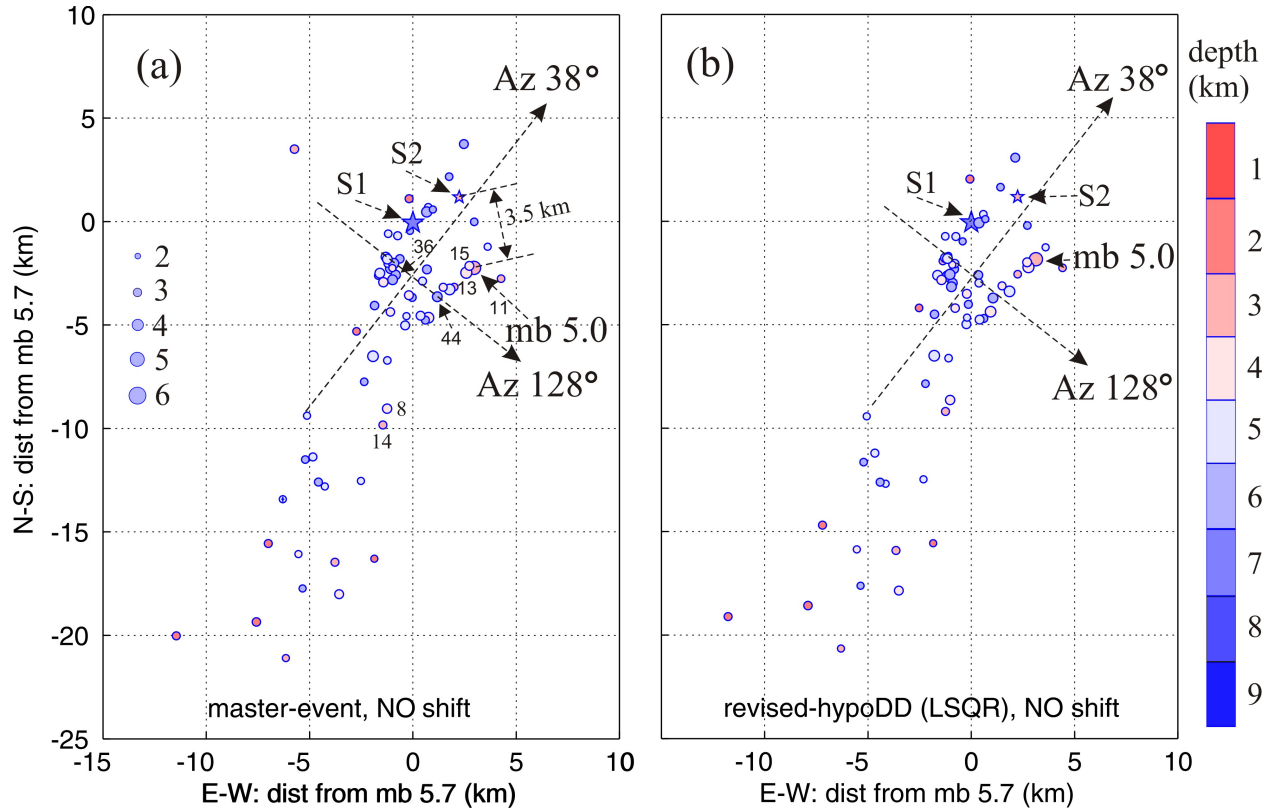


Figure 8. (a) The epicentral distribution of the 68 relocated aftershocks. The size of a solid circle is proportional to the earthquake magnitude, while the color matches the focal depth (see the depth scale on the right). Star S1 marks the center (the location of the mainshock) of the small aftershocks detected in the first field survey, and star S2 marks the center (the location of the mb 5.0 principal aftershock) of the small aftershocks detected in the second survey (Wetmiller et al., 1984). The coordinate point (0, 0) is at (47.0°N; 66.6°W). No. 36 (ME), 44 (SE), 13, 15, 8, and 14 are used in the *An error estimate in the relative locations of epicenters* section. The aftershocks in the upper part of the figure were separated into two groups by a gap region indicated by a dashed-line with an arrow at Az 38°. (b) The epicentral distribution of the 64 aftershocks relocated using the revised-hypoDD. The epicentres in panel (a) were used as the initial input. Among the 68 aftershocks, 64 have epicentral solutions resolved using the LSQR method. This panel is for the *Comparing the relocated epicenters with those by the revised-hypoDD* section.

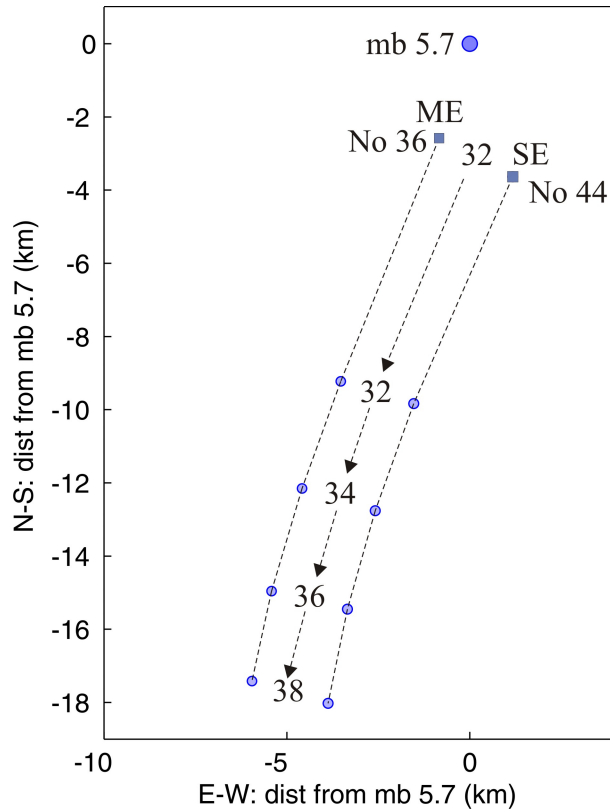


Figure 9.Crustal models and associated epicenters. The solid circle with mb 5.7 represents the epicenter of the mainshock, determined by Wetmiller et al. (1984); the two solid squares with No. 36(ME) and No. 44(SE)represent the relocated epicenters using the crustal model in Figure 5 (thick lines) and a crustal thickness of 32 km. The two solid circles side by side show the same two aftershocks, relocated with the GSC crustal model (Figure 5; dashed lines) and crustal thicknesses of 32, 34, 36, and 38 km, respectively. When the crustal thickness was changed, the two epicenters moved, but their relative positions were visually unchanged.

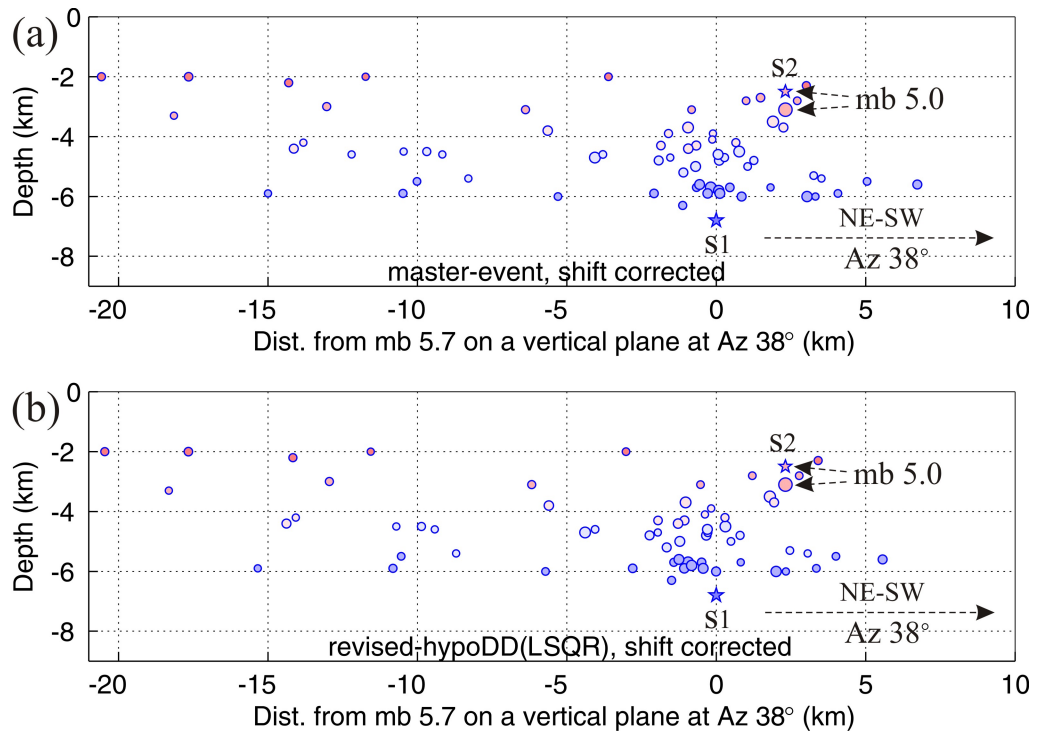


Figure 10. Projections of the shift-corrected hypocenters onto the vertical plane striking at Az 38° (NE–SW) indicated on Figure 8. Most of the aftershocks occurred at depths between 2 km and 6 km. Stars S1 and S2 represent the hypocenter projections of the mainshock and the mb 5.0 aftershock, respectively, obtained by Wetmiller et al. (1984). The size of each solid circle is proportional to the aftershock’s magnitude. (a) Projection of the 68 relocated hypocenters from the master-event method; (b) Projection of the 64 hypocenters relocated using the revised-hypoDD. See section 5.4 for discussion.

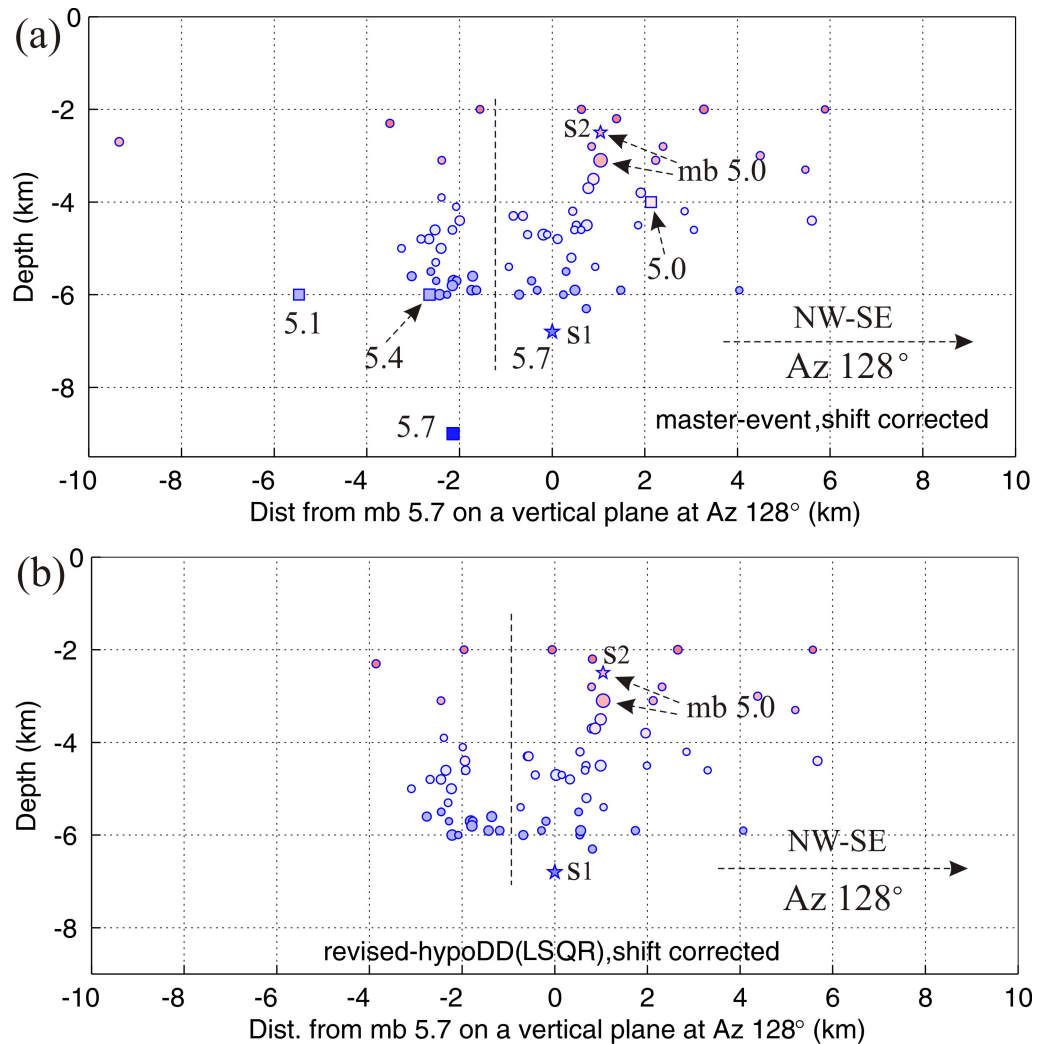


Figure 11. (a) Projection of the 68 relocated hypocenters (the epicenters were shift-corrected) onto a vertical plane, striking at an azimuth of 128° (NW–SE), indicated by a dashed line with an arrow in Figure 8 (a). Most of the aftershocks occurred at depths between 2 km and 6 km. Stars S1 and S2 represent the hypocenter projections of the mainshock and the mb 5.0 aftershock, respectively, obtained by Wetmiller et al. (1984). The size of a solid circle is proportional to the magnitude. The squares, indicated with 5.7, 5.1, 5.4, and 5.0, show the hypocenter projections of the mainshock and its three principal aftershocks, respectively, relocated by Choy et al. (1983). The aftershocks were separated into two groups by a gap region indicated by a vertical dashed line. (b) Projection of the 64 hypocenters relocated using the revised-hypoDD, onto the same vertical plane as (a). This panel is for the *Comparing the relocated*

epicenters with those by the revised-hypoDDsection. The hypocenters on the left side of the vertical line are clustered at depths from about 4 km to 6 km [epicenters are those in the upper-left side of Figure 8 (a)]. Most of the aftershocks occupy a region of around 5×5 km.

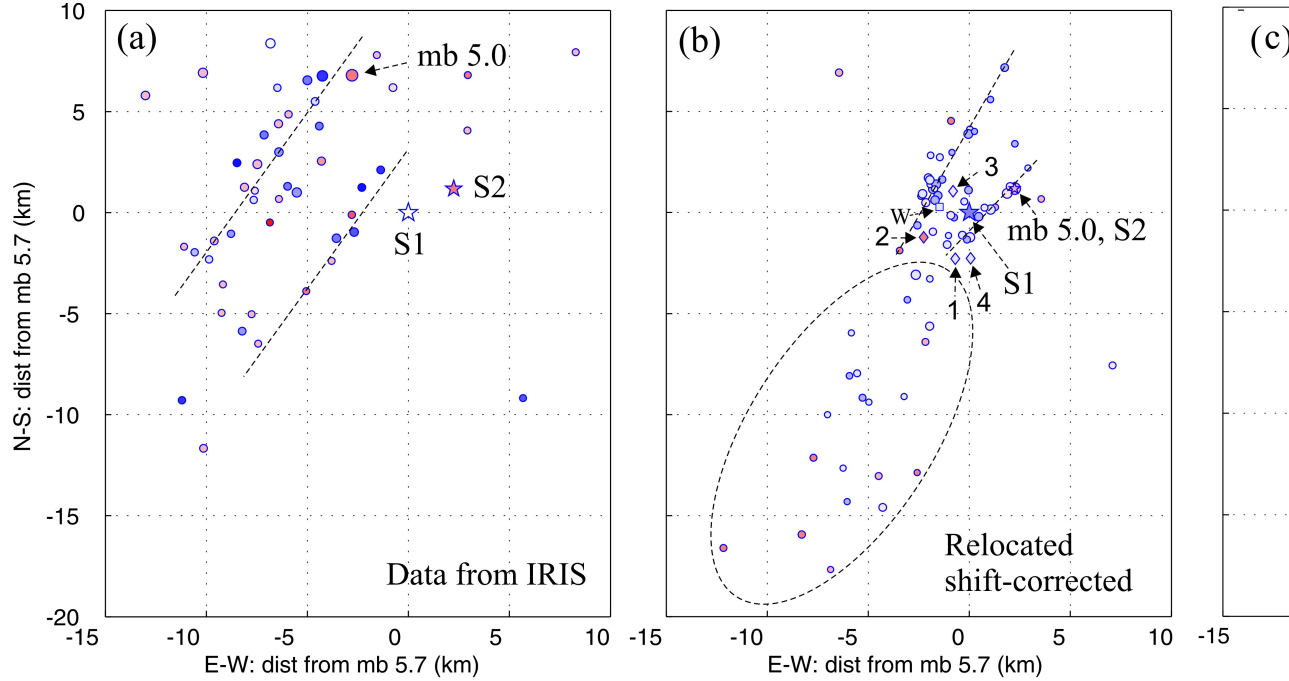


Figure 12. Comparison of epicentral distributions. (a) Plotted using the epicenters obtained by ISC, listed in Table 3. Stars S1 and S2 mark the epicenters of the mainshock and the mb 5.0 aftershock, respectively, determined by Wetmiller et al. (1984). The epicenters are scattered along the northwest side of the mainshock. (b) Plotted using the 68 shift-corrected epicenters. Stars S1, S2, and the square W mark the epicenters of the mainshock, the mb 5.0 aftershock, and a small aftershock, respectively, determined by Wetmiller et al. (1984). The diamonds mark the epicenters relocated by Saikia and Herrmann (1985) for four small aftershocks. Most of the epicenters are around the mainshock. The aftershocks in the dashed oval may indicate the stress adjustment near the source region. Both (a) and (b) show that there are two linear trends in a northeasterly direction. (c) The solid circles show the epicenters of the 40 aftershocks that occurred from 15 to 22 January 1982, located by USGS using a portable digital network, marked with triangles (Cranswick et al., 1982). The four solid squares, indicated with 5.7, 5.1, 5.4, and 5.0, show the epicenters of the mainshock and its three principal aftershocks, respectively, determined by Choy et al. (1983). This panel is for the *Discussion and conclusion* section.

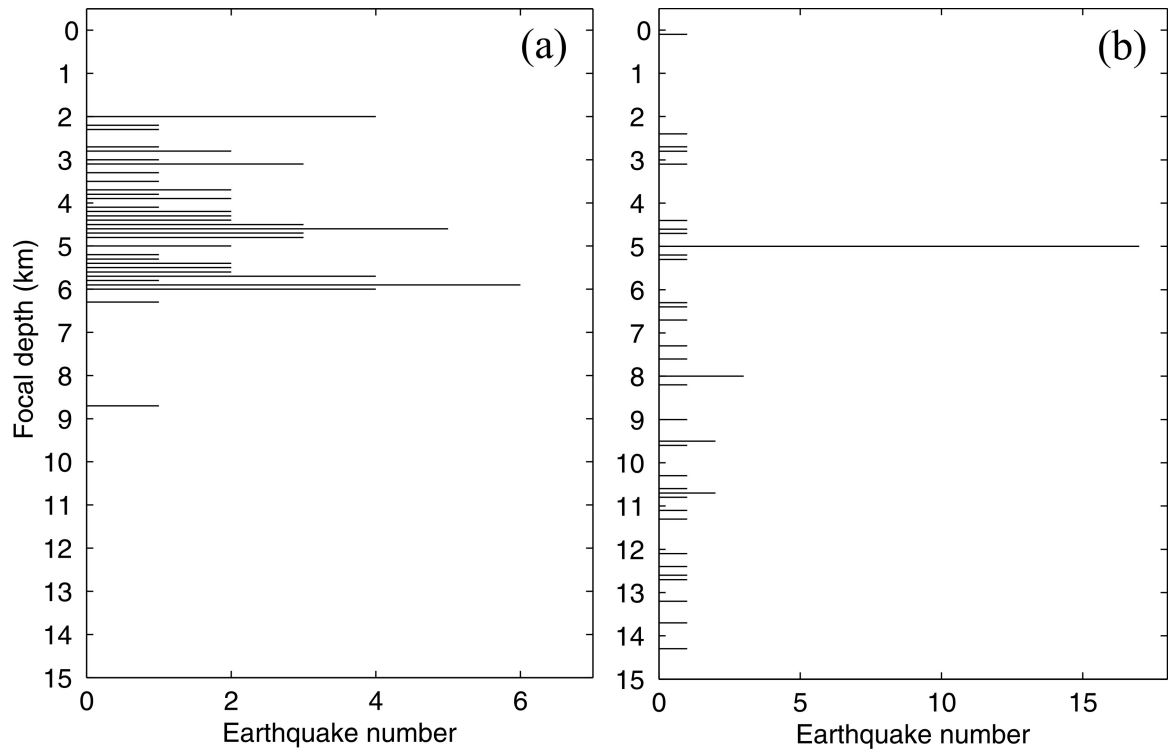


Figure 13. (a) The depthdistribution of the 68 relocated aftershocks. The focal depths range from about 2 km to 6 km. (b) The depth distribution of the aftershocks in Table 3. Ofthe 54 aftershocks, 17 have a nominal depth value of 5 km. The other aftershocks are distributed from the surface to a depth of about 15 km.